

**Optimizing optoelectronic properties of Perovskite
Absorber material via ambient compositional
engineering with Potassium (K) and Tin (Sn)**



By

Muhammad Usman Nawaz

Reg. No. 00000317622

Session 2019-21

Supervised by

Dr. Nadia Shahzad

**US-Pakistan Center for Advanced Studies in Energy
(USPCAS-E)**

National University of Sciences and Technology (NUST)

Islamabad, Pakistan

August 2023

**Optimizing optoelectronic properties of Perovskite
Absorber material via ambient compositional
engineering with Potassium (K) and Tin (Sn)**



**By
Muhammad Usman Nawaz**

Reg. No. 00000317622

Session 2019-21

**Supervised by
Dr. Nadia Shahzad**

**A Thesis Submitted to the US-Pakistan Center for Advanced
Studies in Energy in partial fulfillment of the requirements
for the degree of**

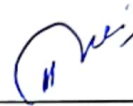
**MASTER of SCIENCE in
Energy Systems Engineering**

**US-Pakistan Center for Advanced Studies in Energy
(USPCAS-E)
National University of Sciences and Technology (NUST)
Islamabad, Pakistan
August 2022**

THESIS ACCEPTANCE CERTIFICATE

Certified that final copy of MS/MPhil thesis written by **Mr. Muhammad Usman Nawaz** having Registration No. **00000317622** of **USPCAS-E** has been vetted by undersigned, found complete in all respects as per NUST Statues/Regulations, is free of plagiarism, errors, and mistakes and is accepted as partial fulfillment for the award of MS/MPhil degree. It is further certified that necessary amendments as pointed out by GEC members of the scholar have also been incorporated in the said thesis.

Signature:




Name of Supervisor

Dr. Nadia Shahzad

Date:

16/08/2023

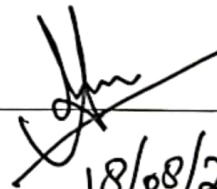
Signature (HoD):



Date:

17/8/2023

Signature (Dean/Principal):



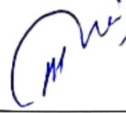
Date:

18/08/2023

Certificate

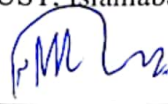
This is to certify that work in this thesis has been carried out by **Mr. Muhammad Usman Nawaz** and completed under my supervision in Solar Energy Research Laboratory, U.S.-Pakistan Center for Advanced Studies in Energy, National University of Sciences and Technology, H-12, Islamabad, Pakistan.

Supervisor:



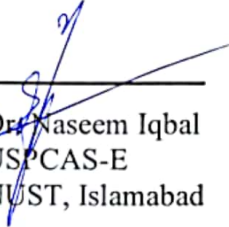
Dr. Nadia Shahzad
USPCAS-E
NUST, Islamabad

GEC member # 1:



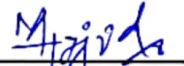
Dr. Muhammad Imran Shahzad
USPCAS-E
NUST, Islamabad

GEC member # 2:




Dr. Naseem Iqbal
USPCAS-E
NUST, Islamabad

GEC member # 3:



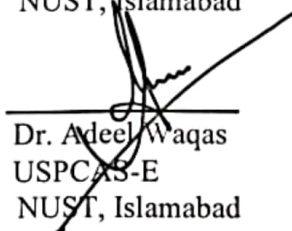
Dr. Majid Ali
USPCAS-E
NUST, Islamabad

HOD-ESE



Dr. Rabia Liaquat
USPCAS-E
NUST, Islamabad

Principal



Dr. Adeel Waqas
USPCAS-E
NUST, Islamabad

Dedication

The research work and thesis are dedicated to my beloved parents who believed in me and prayed for me and my success in every phase of life. I also dedicate this to my friend Muhammad Salik Qureshi for his support, motivation and help throughout this time and always pushing me to do my best. I want to thank for their love and endless support. Even when I was going through tough time in my life, you all have been the reason to push me and proved to a helping hand for me.

Acknowledgment

First and foremost, I would like to express gratitude to Allah (SWT), the Almighty God for the blessing, kindness, and inspiration in lending me to accomplish the research work, Without Him, I couldn't stay patient and in control in this research work.

I express my heartfelt gratitude to my supervisor, Dr. Nadia Shahzad, for her invaluable guidance and support throughout this study, and for believing in my abilities. Her motivation, constant reminders, constructive feedback, and consistent encouragement helped me overcome numerous challenges along the way. I also extend my gratitude to all the faculty and GEC members for their unconditional support. I am thankful especially to my parents, and friends for their encouragement and prayers, which helped me to stay motivated and believe in myself.

Abstract

Perovskite solar cells (PSC) have proved to be an ideal candidate for next-generation photovoltaic technology because of their exceptional light-harvesting properties and cost-effectiveness. Perovskite absorber layer as a heart of the PV cells plays a vital role in determining the overall efficiency of these solar cells but lead toxicity and Sn oxidation are a major hurdle in the way. In this study, we focus on exploring the potential of mixed cation i.e., Sn-Pb based perovskite absorber layers, which have shown significant progress in recent research. Through systematic experimentation, we investigated the influence of doping potassium (K) and tin (Sn) in the A and B sites of MAPbI_3 , respectively, to reduce Sn vacancies and increase the light absorption and film stability. The bandgap bowing has been achieved by successfully incorporating K and Sn in the lattice, enhancing the light absorption capability. Moreover, we used Sn powder as an additive to investigate its role in enhancing the stability of perovskite films. The addition of Sn powder led to a more uniform and high-quality perovskite film, with improved optoelectronic properties. Our research carefully analyzed the role of Sn-Pb based perovskite absorber layers and demonstrates the potential of potassium and tin doping in further improving the performance of perovskite solar cells. The results gathered from this research attempts to advance perovskite technology, opening the way for more efficient and sustainable solar energy harvesting devices.

Keywords: Perovskite solar cells, Sn-Pb based perovskite, potassium and tin doping, compositional engineering, photovoltaic technology, ambient fabrication.

Table of Contents

Chapter 1	1
1.1. Use & Consumption of Fossil fuels:	1
1.2. Adverse Effects of Fossil fuels – Need for more sustainable sources:	3
1.3. Solar Energy – An answer to world energy crises:	4
1.4. Solar Energy	5
1.5. Solar Photovoltaic Cells	6
1.6. Perovskite Solar Cells:	9
1.7. Difficulties facing PSCs:	10
1.8. Advantageous Use of Thin Films and PSCs:	12
1.9. Applications of PSCs:	12
1.10. Problem Statement:	13
1.11. Research Area:	13
1.12. Objectives:	14
Summary:	15
Chapter 2	19
2.1. Crystal Structure of Perovskites:	19
2.2. Compositional Engineering in Perovskite Absorber Layer:	20
2.3. Challenges and Hurdles:	21
2.4. Mixed Cation Perovskites:	23
2.4.1. K-doped MAPbI ₃ :	24
2.5. Use of Sn-powder as an additive:	29
2.6. Delayed annealing of Thin Film:	30
2.7. Research gap and Proposed Solution:	30
Chapter 3	38

Brief detail of Experimental Techniques	38
3.1 Plasma Cleaning	38
3.2 Glove Box:	39
3.3 Spin coater:	41
3.4 Scanning Electron Microscopy	42
3.5 X-ray Diffraction	43
3.6 Fourier Transform Infrared Spectroscopy	44
3.7 UV-vis Spectroscopy:	45
3.8 Photoluminescence	46
Summary	48
References	49
Chapter 4	51
Experimental Work	51
4.1 Materials	51
4.2 Precursor Preparation	51
4.3 Deposition of Perovskite Absorber Layer	52
4.4 Characterization Techniques used with parameters	53
Summary:	54
Chapter 5	55
5.1 Optical microscopy (OM) analysis	55
5.2 SEM and EDS/Mapping analyses	58
5.3 XRD analysis	61
5.4 UV-Vis analysis	63
5.5 PL spectroscopy	66
5.6 Contact angle measurements	68

Chapter 6.....	75
6.1 Conclusion.....	75
6.2 Future Recommendations.....	75

List of Tables

TABLE 2.1: POTASSIUM HALIDE DOPED PEROVSKITE SOLAR CELLS OVER THE YEARS.....	24
TABLE 5.1: STATISTICAL DATA EXTRACTED FROM OM MICROGRAPHS	57

List of Figures

FIGURE 1.1: CONSUMPTION OF FOSSIL FUEL [2]	2
FIGURE 1.2: RENEWABLE ENERGY RESOURCES [4].....	4
FIGURE 1.3: GENERATIONS OF PV SOLAR CELLS [14]	8
FIGURE 1.4: STRUCTURE OF PEROVSKITE SOLAR CELL [15]	10
FIGURE 2.1: CRYSTAL STRUCTURE OF OXIDE PEROVSKITES [4].....	19
FIGURE 2.2: PEROVSKITE STRUCTURE [8]	20
FIGURE 2.3: BANDGAP TUNING OF MIXED Pb-Sn PEROVSKITE SOLAR CELLS.....	21
FIGURE 3.1: PLASMA CLEANER.....	38
FIGURE 3.2: GLOVE BOX.....	40
FIGURE 3.3: SPIN COATER [5]	41
FIGURE 3.4: SCANNING ELECTRON MICROSCOPE [6]	42
FIGURE 3.5: X-RAY DIFFRACTION (XRD) [8]	43
FIGURE 3.6: FOURIER TRANSFORM INFRARED SPECTROSCOPY (FTIR) WORKING STRUCTURE [11].....	45
FIGURE 3.7: WORKING MECHANISM OF UV-VIS SPECTROSCOPY [12]	46
FIGURE 5.1: OPTICAL MICROSCOPE IMAGES OF SOLAR CELLS BASED ON THE FOLLOWING PEROVSKITE PHASE: (A) MAPbI ₃ , (B) MAPbI ₃ DOPED WITH POTASSIUM, (C) MAPbI ₃ DOPED WITH POTASSIUM AND 10% WT. Sn, AND (D) MAPbI ₃ DOPED WITH POTASSIUM AND 20% WT. Sn	55
FIGURE 5.2: SIZE DISTRIBUTION HISTOGRAMS OF SOLAR CELLS BASED ON THE FOLLOWING PEROVSKITE PHASE: (A) MAPbI ₃ , (B) MAPbI ₃ DOPED WITH POTASSIUM, AND (C) MAPbI ₃ DOPED WITH POTASSIUM AND 10% WT. Sn.	56
FIGURE 5.3: SEM MICROGRAPHS OF SOLAR CELLS BASED ON THE FOLLOWING PEROVSKITE PHASE: (A) MAPbI ₃ , (B) MAPbI ₃ DOPED WITH POTASSIUM, (C) MAPbI ₃ DOPED WITH POTASSIUM AND 10 % WT. Sn, AND (D) MAPbI ₃ DOPED WITH POTASSIUM AND 20 % WT. Sn.	58
FIGURE 5.4: (A) EDS AND ELEMENTAL MAPPING RESULTS FOR THE MAPbI ₃ SAMPLE (B) EDS AND ELEMENTAL MAPPING RESULTS FOR THE MAPbI ₃ DOPED WITH POTASSIUM.	59
FIGURE 5.5: (A) EDS AND ELEMENTAL MAPPING RESULTS FOR THE MAPbI ₃ DOPED WITH POTASSIUM AND 10 % WT. Sn (B) EDS AND ELEMENTAL MAPPING RESULTS FOR THE MAPbI ₃ DOPED WITH POTASSIUM AND 20 % WT. Sn.	59

FIGURE 5.6: XRD PATTERNS OF THE METHYLAMMONIUM LEAD IODIDE (S) FILMS BEFORE AND AFTER DOPING PROCESS WITH POTASSIUM (K) AND DIFFERENT CONCENTRATION OF TIN (10 AND 20 % WT.) ELEMENT.....	61
FIGURE 5.7: UV-VIS SPECTRA OF THE METHYLAMMONIUM LEAD IODIDE (S) FILMS BEFORE AND AFTER DOPING PROCESS WITH POTASSIUM (K) AND DIFFERENT CONCENTRATION OF TIN (10 AND 20 % WT.) ELEMENT.....	64
FIGURE 5.8: . TAUC PLOTS OF THE METHYLAMMONIUM LEAD IODIDE (S) FILMS BEFORE AND AFTER DOPING PROCESS WITH POTASSIUM (K) AND DIFFERENT CONCENTRATION OF TIN (10 AND 20 % WT.) ELEMENT.....	64
FIGURE 5.9: FTIR SPECTRA OF THE METHYLAMMONIUM LEAD IODIDE (S) FILMS BEFORE AND AFTER DOPING PROCESS WITH POTASSIUM (K) AND DIFFERENT CONCENTRATION OF TIN (10 AND 20 % WT.) ELEMENT.....	65
FIGURE 5.10: PL SPECTRA OF THE METHYLAMMONIUM LEAD IODIDE (S) FILMS BEFORE AND AFTER DOPING PROCESS WITH POTASSIUM (K) AND DIFFERENT CONCENTRATION OF TIN (10 AND 20 % WT.) ELEMENT.....	67
FIGURE 5.11: CONTACT ANGLE PHOTOGRAPHS BASED ON THE FOLLOWING PEROVSKITE PHASE: (A) MAPbI ₃ , (B) MAPbI ₃ DOPED WITH POTASSIUM, (C) MAPbI ₃ DOPED WITH POTASSIUM AND 10 % WT. SN, AND (D) MAPbI ₃ DOPED WITH POTASSIUM AND 20 % WT. SN	69

List of Publications

1. **Muhammad Usman Nawaz**; Nadia Shahzad; Muhammad Salik Qureshi; Naseem Iqbal; Majid Ali Muhammad Imran Shahzad, *“Optimizing optoelectronic properties of Perovskite Absorber Material via ambient compositional engineering with Potassium (K) and Tin (Sn).”*, Journal of Photochemistry and Photobiology , A: Chemistry (Submitted).
2. Muhammad Salik Qureshi ; Nadia Shahzad; Muhammad Ali Tariq; **Muhammad Usman Nawaz**; Muhammad Imran Shahzad; Salman Riaz, *“Fabrication of HTL free Perovskite Solar Cells using Compositional Engineering via Cesium Bromide for Ambient Fabrication”*, Applied Physics Letters (Submitted).
3. Muhammad Salik Qureshi; Nadia Shahzad; **Muhammad Usman Nawaz**; Saad Nadeem; Sana Mehmood; Abdul Sattar; Sehar Shakir; Naseem Iqbal; Muhammad Imran Shahzad, *“Characterizing the Synergistic Effects of SnO₂-MoS₂ Nanocomposite electron transport layer for perovskite solar cell”* (Submitted).

List of abbreviations

SnI ₂	Tin Iodide
PbI ₂	Lead Iodide
J _{sc}	Short Circuit Current
V _{oc}	Open Circuit Voltage
FF.....	Fill Factor
MA.....	Methylammonium
FA.....	Formamidinium
ETL.....	Electron Transport Layer
HTL.....	Hole Transport Layer
FTO.....	Florine Doped Tin Oxide
PSC.....	Perovskite Solar Cell
PCE.....	Power Conversion Efficiency
ETL.....	Electron Transport Layer
HTL.....	Hole Transport Layer
UV-Vis.....	Ultraviolet Visible
XRD.....	X-Ray Diffraction
SEM.....	Scanning Electron Microscopy
OM.....	Optical Microscopy
PL.....	Photoluminescence

Chapter 1

Introduction

The need for more effective and unconventional energy sources is growing as the world develops quickly. Traditional energy sources have major environmental issues and are running out. The use of thermal energy from the sun by humans' dates to the cave age. More effective techniques to meet the need for energy have been created since the industrial revolution. Photovoltaic solar cells are one such method for harnessing the energy of the sun. The use and effects of traditional energy sources, as well as the potential and continuing research in the field of solar energy, will all be briefly discussed in this chapter.

1.1. Use & Consumption of Fossil fuels:

Fossil fuels have historically been the main source of our energy needs, supporting the expansion and advancement of societies all over the world. Natural gas, coal, and oil have all been used to power homes, businesses, and transportation infrastructure. World fossil fuel consumption has been shown in the figure 1.1. But when these fossil fuels are burned, a lot of greenhouse gases are released into the atmosphere. The main offenders, which contribute to the greenhouse effect and subsequent warming of our planet, are carbon dioxide (CO₂), methane (CH₄), and nitrous oxide (N₂O) [1].

The effects of high emissions of greenhouse gases are substantial and far-reaching. The buildup of these gases in the atmosphere has contributed to global warming and a few alarming environmental impacts. Sea levels have risen because of glaciers and polar ice caps melting because of rising temperatures. The vulnerability of low-lying coastal regions and islands to flooding is growing, endangering populated areas, biodiversity, and essential ecosystems.

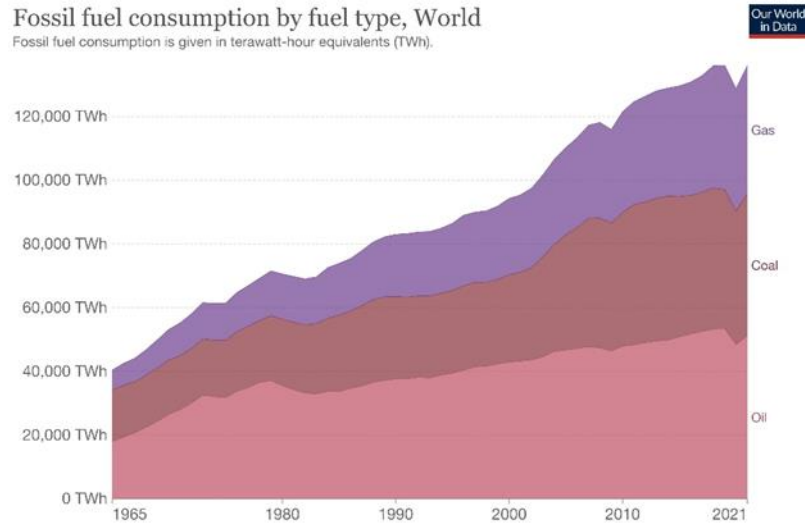


Figure 1.1: Consumption of fossil fuel [2]

In addition, weather patterns have been altered by climate change, which has increased the frequency and severity of extreme weather occurrences. Heatwaves, hurricanes, droughts, and floods have become more frequent and have a devastating effect on infrastructure and populations. Water resources, agriculture, and food production are all negatively impacted, which has serious repercussions for the world's food security [3].

The international community is rapidly embracing the shift toward cleaner and renewable energy sources as a means of addressing the critical need to do so. Solar, wind, and hydropower are examples of renewable energy sources that provide environmentally friendly options with low operational greenhouse gas emissions. This move not only increases energy independence, lowers air pollution, and stimulates economic growth through the production of green technology and jobs, but it also aids in the fight against climate change.

Energy efficiency initiatives, environmentally friendly urban planning, and the adoption of cleaner transportation options are all part of efforts to reduce greenhouse gas emissions. By cutting emissions and fostering international collaboration, international agreements like the Paris Agreement seek to prevent global warming.

In conclusion, the usage of fossil fuels and the subsequent emissions of greenhouse gases have had a significant negative impact on the environment. We must switch to greener, more sustainable energy sources and take action to lessen our carbon footprint. We can lessen the effects of climate change, protect our ecosystems, and build a more sustainable

future for future generations by embracing renewable energy and implementing ecologically responsible habits.

1.2. Adverse Effects of Fossil fuels – Need for more sustainable sources:

The negative effects of using fossil fuels are widespread and necessitate a swift transition to renewable energy sources, with a focus on solar energy gathering. Fossil fuel combustion results in significant atmospheric emissions of greenhouse gases like carbon dioxide. These gases trap heat and aid in global warming, which has several negative effects. As a result of melting glaciers and polar ice caps brought on by a rise in global temperatures, coastal communities and ecosystems are at serious risk.

The rising amount of greenhouse gases disrupts weather patterns and intensifies extreme events like hurricanes, droughts, and floods, affecting human life, infrastructure, and agriculture. Fossil fuel combustion produces air pollutants, leading to respiratory and cardiovascular health issues for both humans and wildlife. Using renewable energy sources is necessary to stop climate change. A pure, plentiful, and emission-free energy source that lowers the carbon footprint is solar energy. Through the conversion of sunlight into electricity, solar panels present a sustainable alternative. Figure 1.2 shows the various renewable energy sources available.

Due to its vast availability, solar energy also supports energy resilience and independence. In order to improve energy security during natural catastrophes and blackouts, distribution of energy generation through rooftop and community solar systems reduces reliance on centralized power networks and fossil fuels. To advance sustainability and lessen the effects of climate change, solar technology must be adopted. [5]

Economic expansion and job creation are also fueled by the adoption of solar energy harvesting. Jobs in production, installation, maintenance, and research and development are available in the solar business. In addition to lowering greenhouse gas emissions, the ongoing development of solar energy infrastructure boosts regional economies, encourages innovation, and places nations at the forefront of clean energy technologies. [6] [4]

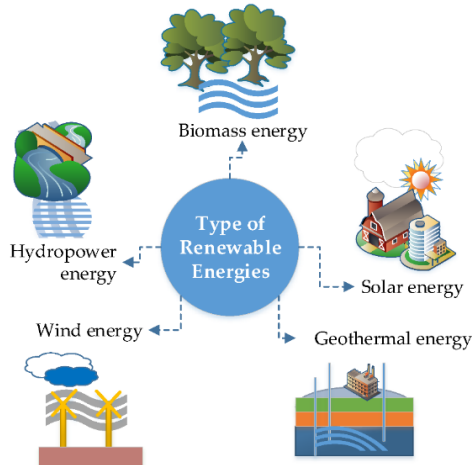


Figure 1.2: Renewable Energy Resources [4]

In conclusion, switching to renewable energy sources is necessary to mitigate the negative consequences of fossil fuel use, with solar energy collection being a key component. A clean, abundant, and sustainable alternative to fossil fuels, solar power helps to reduce climate change, enhance air quality, and encourage energy independence. We can address the urgent issues caused by the use of fossil fuels and pave the way for a sustainable and resilient future by embracing solar energy and investing in its continued development and use.

1.3. Solar Energy – An answer to world energy crises:

Solar energy offers a compelling solution to energy shortages, providing environmental advantages and significant economic benefits. Investing in solar infrastructure comes with low operating costs due to abundant and free sunlight, reducing reliance on expensive fuel imports. The stable and predictable energy supply of solar power enables better long-term financial planning compared to fluctuating conventional energy costs. Technological advancements have made solar technology cost-competitive, evident in its lower levelized cost of energy (LCOE) over time. Furthermore, solar energy installations can result in cost savings through net metering and feed-in tariff programs. Surplus electricity generated by solar systems can be sold back to the grid, offsetting energy expenses. Solar energy usage also stimulates the economy and creates job opportunities in the renewable energy sector. With long lifespans and potential income generation through

surplus electricity sales, investing in solar energy promises financial sustainability and offers a practical and environmentally friendly energy solution.

Overall, the financial and economic advantages of solar energy make it an appealing response to energy shortages. Low operating costs, protection from varying fuel prices, the creation of jobs, chances for financial savings, and long-term returns on investment are some of its benefits. Countries and communities can attain environmental sustainability and economic prosperity by embracing solar electricity.

1.4. Solar Energy

Solar energy is a renewable and non-conventional source of energy in which sun's energy is harvested. Given that it doesn't produce damaging greenhouse gases or contribute to air pollution, its clean and sustainable nature makes it a possible replacement for fossil fuels. Solar energy's adaptability makes it possible to use it in a variety of ways to satisfy our energy demands, providing a greener and more sustainable future. [7]

The potential for solar energy is enormous; it is believed that the Earth receives 173,000 terawatts of solar energy per year, which is 10,000 times more than what the entire world consumes in energy. The efficiency of capturing solar energy has increased as a result of technological improvements. Some solar panels currently have conversion efficiencies of over 20%, while new technologies like perovskite and thin-film solar cells offer advantages in terms of cost and application versatility. [8]

Given that the Sun will continue to emit energy for billions of years, solar energy is a sustainable and renewable source of energy. Solar irradiance is the term used to describe the quantity of solar energy that reaches the Earth's surface. The amount of electromagnetic energy that is received from the Sun per square meter is known as solar irradiance. Watts per square meter (W/m^2) is the unit of measurement. Based on variables such the time of day, location, season, and meteorological conditions, the solar irradiance at the Earth's surface changes. The sun irradiation can reach approximately $1000 \text{ W}/\text{m}^2$ at noon on a clear day. [9]

There are two primary ways to harness solar energy: photovoltaic (PV) technology and solar thermal technology.

- a. Photovoltaic (PV) Technology: Silicon-based semiconductors are used to create PV cells, also referred to as solar cells. Electrons in the semiconductor are excited by photons in the sunshine as they hit the PV cells, producing an electric current. Solar panels that produce electricity for buildings, companies, and power grids rely on this direct conversion of sunlight into electricity as their primary energy source.
- b. Solar Thermal Technology: Solar thermal systems harness the energy of the Sun to generate electricity, heat water, and space. Mirrors or lenses are used in concentrated solar power (CSP) facilities to focus sunlight onto a receiver, which heats a working fluid to produce steam that powers turbines and produces electricity. Solar water heaters reheat water for a variety of uses by utilizing the Sun's heat.

The quality of solar panels or thermal collectors, solar irradiance, temperature, and system design are some of the variables that affect how well solar energy is converted. The effectiveness and affordability of solar energy systems continue to increase because to research and technological advancements. In conclusion, solar energy is an important and promising resource that provides a long-term and sustainable answer to our expanding energy needs. Both photovoltaic and solar thermal energy harvesting show enormous promise for the transition to a cleaner and more sustainable energy future. [10], [11]

1.5. Solar Photovoltaic Cells

Since its invention and early development, photovoltaic (PV) technology has made amazing strides. The initial recording of the photovoltaic effect, made in 1839 by French physicist Alexandre-Edmond Becquerel, is considered to represent the beginning of PV technology. He found that some substances generated an electric current when exposed to light. However, significant progress was not achieved in harnessing this phenomenon for useful uses until the middle of the 20th century.

The first usable silicon solar cell was created in the 1950s by Bell Laboratories researchers Gerald Pearson, Calvin Fuller, and Daryl Chapin. This innovation made it possible for PV technology to be commercialized. The silicon solar cell showed more stability and efficiency, making it an effective choice for producing power from sunshine. Research efforts in the ensuing decades were concentrated on raising the effectiveness and affordability of solar cells. To improve the conversion of sunlight into power, scientists investigated numerous materials and cell designs. Due to its availability, dependability, and

efficiency, silicon has remained the predominant material. There have been several generations of solar cells created, such as monocrystalline, polycrystalline, and thin-film cells, each with advantages and disadvantages.

Solar panels were used to power satellites and other spacecraft thanks to breakthroughs in PV technology, which prompted its widespread adoption. The 1970s oil crisis further encouraged research and investment in solar energy as a substitute for fossil fuels, leading to increased effectiveness and lower production costs [12].

Recent research has concentrated on pushing solar cells' efficiency boundaries and investigating novel materials and methods. Multi-junction solar cells are being developed in an effort to capture a wider spectrum of sunlight, including high-energy photons. Due to its potential for low-cost manufacture and flexibility, thin-film solar cells composed of cadmium telluride (CdTe) or copper indium gallium selenide (CIGS) have attracted attention.

Scientists and researchers have been experimenting with new materials and methods to increase the effectiveness, affordability, and adaptability of solar cells. Amorphous silicon, cadmium telluride, and copper indium gallium selenide (CIGS) were some of the alternative materials used in the second-generation solar cells, which included thin-film solar cells. Due to the decreasing material and production costs of these cells, solar energy became more commercially viable. Figure 1.3 illustrates the different generations of PV.

The third generation of solar cells has evolved, building on these developments and emphasizing cutting-edge materials and designs to get beyond the drawbacks of earlier generations. Third-generation solar cells are designed to increase performance, lower costs, and open up new applications. In this generation, a number of potential strategies are being investigated. Utilizing several layers of various materials, such as tandem solar cells, is one method used in the third generation. These cells combine a number of semiconductors with varied energy band gaps in order to absorb a larger range of sunlight and boost overall performance. Organic photovoltaic (OPV) cells, which use organic materials to absorb and transform sunlight into power, are another intriguing option. OPV cells benefit from low manufacturing costs, versatility, and the ability to be integrated into a variety of surfaces and objects [13].

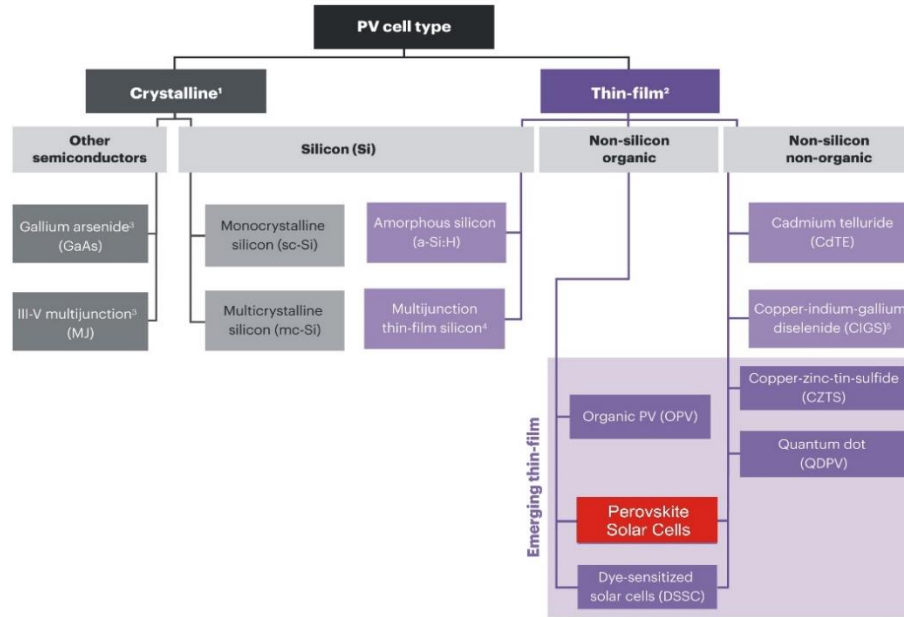


Figure 1.3: Generations of PV Solar Cells [14]

Additionally, research is being done on dye-sensitized solar cells (DSSCs) as a potential third generation solution. In DSSCs, sunlight is absorbed by a dye, and the excited electrons are then transferred to a conductive substance, where they are used to produce electricity. These cells can be used on windows, building facades, and other surfaces and offer the benefit of transparency. Perovskite solar cells have also attracted a lot of attention recently. Perovskite materials can be manufactured at lower temperatures and have high light absorption qualities, which may cut production costs. The goal of ongoing research is to increase the stability and toughness of perovskite solar cells for industrial use.

Additionally, new opportunities for improving PV performance have been made possible by advances in nanotechnology. With the potential for increased efficiency and cheaper production costs, perovskite solar cells and nanostructured materials have demonstrated encouraging results. Researchers are also investigating novel strategies, like tandem solar cells, which combine various materials to maximize light absorption and conversion.

Overall, since its invention, the field of solar technology has advanced significantly. Continual investment in research and development has led to greater applications, lower costs, and more efficiency. Photovoltaic technology is positioned to play a critical part in

meeting the world's energy needs and reducing climate change because to continual developments and the growing appreciation of the value of renewable energy.

1.6. Perovskite Solar Cells:

Perovskite solar cells operate based on a multilayer structure as shown in figure 1.4, that facilitates the efficient conversion of sunlight into electricity. The working mechanism of each layer can be described as follows:

- a. Transparent Conductive Oxide (TCO) Layer: The TCO layer functions as the front electrode of the solar cell and is commonly comprised of materials like indium tin oxide (ITO) or fluorine-doped tin oxide (FTO). While offering a conductive surface to gather the holes (positive charges) produced in the perovskite layer, it is transparent to let sunlight pass through.
- b. Hole-Transporting Layer (HTL): The HTL is a key element that makes it easier for positive charges (holes) to be transported from the perovskite layer to the front electrode. Due to their high conductivity and acceptable energy levels, organic materials, such as Spiro-OMeTAD (2,2',7,7'-tetrakis(N,N-di-p-methoxyphenylamine)-9,9'-spirobifluorene), are frequently utilized as hole-transporting materials.
- c. Perovskite Layer: The perovskite layer, which consists of a thin film of hybrid organic-inorganic perovskite material, is the solar cell's beating heart. Exciton is produced as a result of this layer's absorption of solar photons. Organic cations like methylammonium or Formamidinium and inorganic metal halide ions like lead or tin combined with iodine, bromine, or chlorine make up the majority of the perovskite substance. The production of positively charged holes and the excitation of electrons occur as a result of photon absorption in the perovskite layer.
- d. Electron-Transporting Layer (ETL): The ETL is positioned between the perovskite layer and the back electrode and is frequently made of materials like titanium dioxide (TiO₂) or tin oxide (SnO₂). Its function is to effectively move the produced electrons from the perovskite layer to the back electrode with the least amount of electron recombination with the holes. In order to avoid charge recombination at the interface with the HTL, the ETL also functions as an electron-blocking layer.

- e. Back Electrode: The back electrode acts as the contact for gathering the electrons produced in the perovskite layer and is often comprised of a metal like gold or silver. It offers an electrically conductive channel for electrons to travel on their way to the external circuit [16], [17].
- f. Sunlight penetrates the perovskite layer when it passes through the transparent front electrode. The photons are absorbed by the perovskite material, which excites electrons in the valence band to move into the conduction band and form electron-hole pairs (excitons). After then, the electron-hole couples separate, with the electrons going in the direction of the ETL and the holes moving in the direction of the HTL. The corresponding transport layers make it easier for charges to travel efficiently towards the front and rear electrodes, where they are gathered and used to create an electric current. It is possible to use this current to power external devices or to store it for later use.

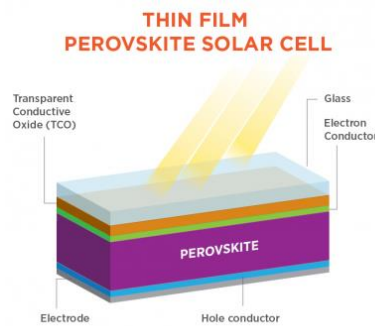


Figure 1.4: Structure of Perovskite Solar Cell [15]

In sum, the distinct arrangement of layers in perovskite solar cells allows for the absorption of sunlight, effective charge separation, and collecting of produced electrons and holes, ultimately producing usable electrical energy. The performance and commercial feasibility of perovskite solar cells are being improved by ongoing research that focuses on enhancing the stability and efficiency of each layer and optimizing the overall device architecture.

1.7. Difficulties facing PSCs:

Perovskite solar cells have attracted a lot of interest in the scientific community, but they also have a number of issues that need to be resolved. As perovskite materials are particularly susceptible to moisture, oxygen, and light, which can damage their performance

over time, guaranteeing their long-term stability is a critical concern. To increase stability and prevent degradation, effective encapsulation methods and improved material compositions are being investigated.

The high lead level that is present in many perovskite materials is a source of additional worry. The commercialization of perovskite solar cells faces considerable obstacles due to the potential toxicity and environmental effects of lead. Lead-free options that maintain high efficiency while addressing health and environmental concerns are currently being intensively researched. [18]

Perovskite solar cell manufacture scaling up is a difficult task. Although laboratory-scale systems have demonstrated excellent efficiency, scaling up these results remains a technical challenge. For commercial viability, it is essential to deposit high-quality, uniform-property perovskite films over a large region. [19]

For perovskite solar cells to be widely used, performance must be repeatable and consistent. Inconsistent efficiency between devices and batches can be caused by variations in film morphology and interface engineering. To produce accurate and repeatable outcomes, efforts are being made to comprehend and regulate these variables.

Perovskite solar cells must meet certain criteria in order to be commercially viable, including cost reduction and environmental sustainability. Research is being done on improving energy conversion efficiency, developing scalable, environmentally friendly manufacturing processes, and optimizing material use. Extending the operational lifetime of perovskite solar cells also requires enhancing device lifetime and reducing degradation mechanisms. [20]

Interdisciplinary partnerships between scientists, engineers, and industry stakeholders are necessary to address these difficulties. To overcome these challenges, more developments in materials, device topologies, manufacturing procedures, encapsulation methods, and fundamental physics of perovskite solar cells are essential. Perovskite solar cells can realize its full potential as a workable and long-lasting photovoltaic technology that contributes to a cleaner and more energy-efficient future by solving these difficulties.

1.8. Advantageous Use of Thin Films and PSCs:

The solar energy industry can benefit from the cost-saving features of perovskite solar cells and thin film solar cells. They require fewer active material layers, which lowers production and material costs. In addition, they can use flexible substrates, which are less expensive than rigid silicon wafers.

Costs for labor and equipment are decreased through scalable manufacturing processes like roll-to-roll printing, spray coating, and vapor deposition. Continuous study attempts to raise their effectiveness, boost energy output, and cut system expenses as a whole. Stability and durability improvements lower maintenance and replacement costs. They are less expensive to assemble and install since they may be spread out over huge areas. Furthermore, they may be seamlessly integrated into surfaces thanks to their architectural adaptability, which negates the need for additional infrastructure.

The overall cost of solar energy generation can be significantly decreased by utilizing the benefits of thin film and perovskite solar cells, such as material efficiency, affordable manufacturing processes, flexible substrates, performance improvement potential, large-area deposition, and design flexibility. These developments hasten the transition to a clean and sustainable energy future by making solar power more widely available, economically viable, and accessible.

1.9. Applications of PSCs:

Beyond the usual solar energy generation, perovskite solar cells have a wide range of applications. They can generate power while preserving the structure's aesthetic appeal by being incorporated into building components like windows, facades, and roofs. Additionally, they are suitable for portable and wearable electronics like backpacks, cellphones, and smartwatches due to their flexibility and light weight, which allows for on-the-go power generation. Perovskite solar cells are useful for off-grid applications as well, enabling distant places with insufficient access to electricity by supplying long-lasting and affordable power for lighting systems and small appliances. Additionally, its incorporation into moving objects like drones, electric boats, and autos can improve energy efficiency and lower greenhouse gas emissions. In larger-scale applications, perovskite solar cells can be utilized

in solar farms and power plants to generate grid-connected electricity, contributing to the renewable energy transition.

Perovskite solar cells have the capacity to generate energy in a variety of situations. Batteries are not necessary because they can use indoor or ambient lighting to power small electronic devices or sensors. They also show promise in cutting-edge fields like perovskite tandem solar cells, which combine multiple layers for greater efficiency. Additionally used in perovskite-based optoelectronic devices including LEDs, photodetectors, and lasers, perovskite solar cells provide effective and affordable solutions. The goal of ongoing research and development in this area is to open up new possibilities and increase the use of perovskite solar cells in sectors and businesses looking for novel and sustainable energy sources.

1.10. Problem Statement:

Lead toxicity, degradation issues and layer efficiency are the primary concerns while working with PSC's. Compositional engineering to partially replace Pb with Sn while keeping the stability intact is a challenge. The use of additives to cope up with the problem of pin holes and to cease the readily oxidation of Tin. A more efficient perovskite absorber layer with mixed cations is the primary focus for applications in Perovskite solar cells as well as tandem cells.

1.11. Research Area:

The aim of this research is to investigate the synthesis and characterization of mixed Pb-Sn based perovskite absorber layer for photovoltaic applications. Although lead-based perovskite materials have shown remarkable efficiency, concerns regarding their toxicity and environmental impact necessitate the exploration of lead-free alternatives. The incorporation of tin (Sn) into the perovskite structure offers a potential solution. However, the synthesis and characterization of mixed Pb-Sn perovskite absorber layers pose challenges due to the complex crystal structure and potential phase segregation. This research aims to overcome these challenges by developing optimized synthesis methods and characterizing the structural, optical, and electrical properties of the resulting mixed Pb-Sn perovskite absorber layers. The goal is to achieve high-performance, environmentally

friendly perovskite solar cells through the development of efficient and stable mixed Pb-Sn perovskite materials.

1.12. Objectives:

The focus of the research includes the following objectives:

- a. Enhanced Stability: Compositional Engineering of conventional Perovskite absorber layer MAPbI_3 and partial doping of cations in the site A and B.
- b. Characterizations: Conduct thorough structural, morphological and optical of the perovskite layer to understand its properties and performance.
- c. Stability-Performance Tradeoff: Investigate the relationship between stability and performance by studying different fabrication techniques, material compositions, and device architectures.

By achieving these objectives, the aim is to contribute to the development of stable and efficient perovskite-based photovoltaic and optoelectronic devices with wider applicability.

Summary:

This chapter emphasizes the significance of solar photovoltaic (PV) technology as a solution to the adverse effects of fossil fuel consumption and the need for more sustainable energy sources. The industrial revolution has disrupted the delicate ecosystem balance, resulting in climate change, global warming, and environmental degradation. Solar PV technology offers a clean and abundant alternative, reducing greenhouse gas emissions, promoting energy independence, and fostering economic growth. The chapter also highlights the challenges and opportunities in the field, including the development of perovskite solar cells and their applications in various sectors. The research aims to enhance stability, characterize mixed Pb-Sn perovskite absorber layers, and explore future prospects, contributing to the advancement of solar energy technologies.

References

- [1] K. Bithas and P. Kalimeris, “A Brief History of Energy Use in Human Societies,” pp. 5–10, 2016, doi: 10.1007/978-3-319-20732-2_2/COVER.
- [2] H. Ritchie, M. Roser, and P. Rosado, “Energy,” *Our World in Data*, Oct. 2022, Accessed: Jul. 18, 2023. [Online]. Available: <https://ourworldindata.org/energy>
- [3] J. Edmonds and J. Reilly, “A long-term global energy- economic model of carbon dioxide release from fossil fuel use,” *Energy Econ*, vol. 5, no. 2, pp. 74–88, Apr. 1983, doi: 10.1016/0140-9883(83)90014-2.
- [4] R. Avtar *et al.*, “Exploring Renewable Energy Resources Using Remote Sensing and GIS—A Review,” *Resources 2019, Vol. 8, Page 149*, vol. 8, no. 3, p. 149, Aug. 2019, doi: 10.3390/RESOURCES8030149.
- [5] V. Marano, M. Muratori, G. Rizzo, and G. Rizzoni, “Electric Mobility: from Fossil Fuels to Renewable Energy, Opportunities and Challenges,” *IFAC Proceedings Volumes*, vol. 46, no. 21, pp. 812–817, Jan. 2013, doi: 10.3182/20130904-4-JP-2042.00161.
- [6] V. Smil, “Global Warming and Future Fossil Fuel Consumption,” *Energy Studies Review*, vol. 1, no. 2, Dec. 1989, doi: 10.15173/ESR.V1I2.184.
- [7] B. Das and Jagadish, “Introduction,” pp. 1–22, 2023, doi: 10.1007/978-3-031-27635-4_1.
- [8] R. Riswan, “Fundamentals of Renewable Energy Processes.pdf.” Accessed: Jul. 18, 2023. [Online]. Available: https://www.academia.edu/29663981/Fundamentals_of_Renewable_Energy_Processes_pdf
- [9] International Renewable Energy Agency (IRENA), “FUTURE OF SOLAR PHOTOVOLTAIC Transformation paper About IRENA,” 2019, Accessed: Jul. 18, 2023. [Online]. Available: www.irena.org/publications.

- [10] M. A. Green *et al.*, “Solar cell efficiency tables (version 62),” *Progress in Photovoltaics: Research and Applications*, vol. 31, no. 7, pp. 651–663, Jul. 2023, doi: 10.1002/PIP.3726.
- [11] S. Yang, W. Fu, Z. Zhang, H. Chen, and C. Z. Li, “Recent advances in perovskite solar cells: efficiency, stability and lead-free perovskite,” *J Mater Chem A Mater*, vol. 5, no. 23, pp. 11462–11482, Jun. 2017, doi: 10.1039/C7TA00366H.
- [12] L. M. Fraas, “History of Solar Cell Development,” *Low-Cost Solar Electric Power*, pp. 1–12, 2014, doi: 10.1007/978-3-319-07530-3_1.
- [13] J. Yan and B. R. Saunders, “Third-generation solar cells: a review and comparison of polymer:fullerene, hybrid polymer and perovskite solar cells,” *RSC Adv*, vol. 4, no. 82, pp. 43286–43314, Sep. 2014, doi: 10.1039/C4RA07064J.
- [14] “ETI Factbook | Solar Photovoltaic - Energy Transition Institute - Kearney.” <https://www.energy-transition-institute.com/insights/solar-photovoltaic> (accessed Jul. 18, 2023).
- [15] T. D. Siegler *et al.*, “The Path to Perovskite Commercialization: A Perspective from the United States Solar Energy Technologies Office,” *ACS Energy Lett*, vol. 7, no. 5, pp. 1728–1734, May 2022, doi: 10.1021/ACSENERGYLETT.2C00698.
- [16] M. A. Green and A. Ho-Baillie, “Perovskite Solar Cells: The Birth of a New Era in Photovoltaics,” *ACS Energy Lett*, vol. 2, no. 4, pp. 822–830, Apr. 2017, doi: 10.1021/ACSENERGYLETT.7B00137/ASSET/IMAGES/MEDIUM/NZ-2017-00137A_0007.GIF.
- [17] N. G. Park, “Halide perovskite photovoltaics: History, progress, and perspectives,” *MRS Bull*, vol. 43, no. 7, pp. 527–533, Jul. 2018, doi: 10.1557/MRS.2018.152.
- [18] J. Bisquert, Y. Qi, T. Ma, and Y. Yan, “Advances and obstacles on perovskite solar cell research from material properties to photovoltaic function,” *ACS Energy Lett*, vol. 2, no. 2, pp. 520–523, Feb. 2017, doi: 10.1021/ACSENERGYLETT.7B00085/ASSET/IMAGES/LARGE/NZ-2017-00085W_0001.JPEG.

[19] Y. Rong *et al.*, “Challenges for commercializing perovskite solar cells,” *Science* (1979), vol. 361, no. 6408, Sep. 2018, doi: 10.1126/SCIENCE.AAT8235/ASSET/DABCEE82-83D5-4237-B932-A2989EAA076D/ASSETS/GRAPHIC/361_AAT8235_F4.JPEG.

[20] S. M. Hasnain, “Examining the advances, obstacles, and achievements of tin-based perovskite solar cells: a review,” *Solar Energy*, vol. 262, p. 111825, Sep. 2023, doi: 10.1016/J.SOLENER.2023.111825.

Chapter 2

Literature Review

2.1. Crystal Structure of Perovskites:

Perovskites are characterized by their general formula ABX_3 and have a cubic structure. Most common classification of perovskites include the traditional oxide perovskites and the other one is organic inorganic Perovskites.

In the world of perovskite structures, the family of oxide perovskites is a key participant. The overall description of these perovskites is given by the formula ABO_3 , where A typically denotes an alkaline or rare earth metal cation present in the oxygen sublattice's 12-fold coordinated cuboctahedra cages. B stands for a transition-metal cation that is coordinated with six oxygen atoms in an octahedral structure. Examples of such cations are Fe, Ni, Mn, Co, Cu, or Ti. [1] But because the ionic size ratios between the various A, B, and O sites inside the crystal frequently deviate from ideal values, the perovskite structure frequently displays aberrations. Some of common TCO's are Strontium Titanate ($SrTiO_3$), Barium titanate ($BaTiO_3$) and Bismuth Ferrite ($BiFeO_3$) [2].

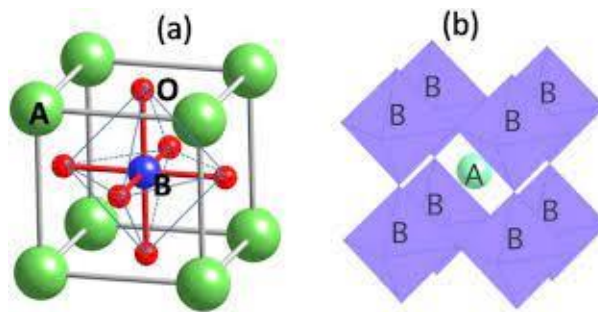


Figure 2.1: Crystal structure of Oxide Perovskites [4]

Additionally, the size and valence of the A or B cations may differ, resulting in oxygen non-stoichiometry. Crystal structure of TCO is shown in the figure 2.1. Both oxygen excess and/or oxygen deficiency must exist within the perovskite structure for this to occur. The distinctive qualities and functions of oxide perovskites are a result of these differences

in size and valence, making them an exciting topic of study in solid-state physics and materials science [3].

On the other hand, we have Hybrid Organic Inorganic Perovskite Solar Cells (PSC's). In the cubic structure, corners are occupied by monovalent cations whereas the divalent cations are found at the body center of the cube. Moreover, the anions are situated in the face center and have -1 oxidation state. In a three-dimensional structure they acquire an octahedral structure. The structure of perovskite can be best described by the Goldschmidt tolerance factor t [5].

$$t = \frac{R_A + R_X}{\sqrt{2}(R_B + R_X)} \approx 1$$

R_A , R_B and R_X correspond to relative radii of cations and anions in the crystal lattice. According to the equation, the size of A cation must be relatively larger than that of B to hold the cubic structure in the crystal lattice.[6] Figure 2.2 shows the perovskite structure. That is the reason methylammonium (CH_3NH_3) is considered an ideal cation in the case of MAPbI_3 structure because the ionic radius of CH_3NH_3 is larger than that of Pb. Methylammonium Lead Iodide (MAPbI_3) exhibits a bandgap of 1.55 eV due to which they are the most used. [7]

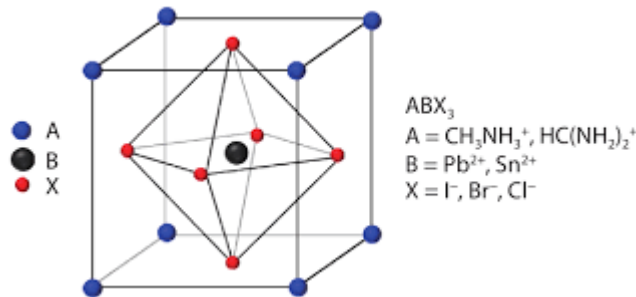


Figure 2.2: Perovskite structure [8]

2.2.Compositional Engineering in Perovskite Absorber Layer:

Mixed halide and mixed Cations Perovskite Solar cells have gained much attention in the last few decades. Since they have a high light absorption coefficient, remarkable optical properties, and flexible bandgap tuning, much of the research is done in this field.

MAPbI₃ has a direct bandgap of 1.5eV whereas MAPbBr₃ and MAPbCl₃ have 2.3eV and 3.11eV. Due to their high bandgap, they have extensive applications in tandem solar cells. [7]

On the other hand, Pb can be replaced by Sn to lower the bandgap. Some of the possible alternatives for Pb are transition metals Cu, Mn, Fe and Co but due to their smaller ionic radius the structure mitigates towards a layered formation. However, Sn has proved to

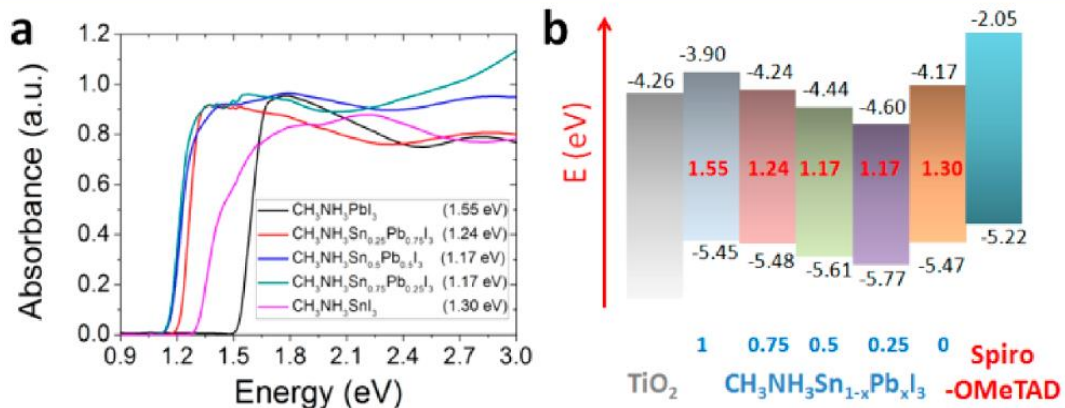


Figure 2.3: Bandgap tuning of Mixed Pb-Sn Perovskite Solar cells.

be the best possible alternative in this case. A lot of research has been done for lead free or Pb-Sn based perovskite solar cells having an ideal bandgap of 1.1 to 1.3 eV illustrated in the figure 2.3 below. [9]

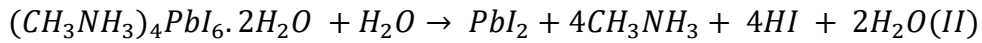
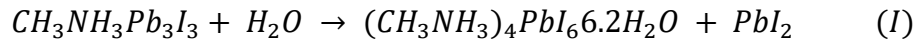
On the A site, other commonly used cation is Formamidinium (FA) which is slightly larger in size than Methylammonium (MA) shrinks the bandgap to 1.48 eV. Other alternatives for MA are Cs and K. Cs based PSC's have shown a bandgap of 1.5 to 1.8 eV. Cs doped perovskites like CsPbI₃ and CsPbBr₃ have shown promising optoelectrical properties and have a bandgap of approximately 1.7 eV. Potassium (K) doped perovskites on the other hand, have a bandgap ranging from 1.1 to 1.6 eV. Potassium is doped to increase the stability and optoelectrical properties of PSC's. [10]

2.3. Challenges and Hurdles:

MAPbI₃ shows promising results in PV but it also have some problems. Pb being a major component of it is highly toxic element. Lead toxicity is an important environmental and health concern as lead can enter the body through inhalation, touch, or injection. Pb

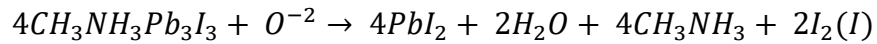
presence in PSC poses a great challenge during production, use and even after disposal. To mitigate the issue either lead free devices like CsSnI₃ should be used or perfect encapsulation is the way.

Another challenge is the stability of the Pb based solar cell. Pb is a heavy element that is highly unstable in the presence of oxygen and water. This causes the degradation of the cell and decrease the lifecycle. Upon reacting with water, MAPbI₃ forms Lead iodide and hydrate complex as shown in the in equation I, which again reacts with moisture and produce Hydrogen Iodide in equation II.



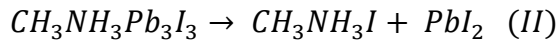
RH of 50% will degrade the device in almost 10 days and this will increase rapidly in the presence of 80% RH. [7]

Perovskite films are susceptible to degradation from oxygen and light exposure. When oxygen diffuses into the perovskite crystal, it reacts with iodine vacancies, forming highly reactive O²⁻ ions. As a result, the photo-excited perovskite undergoes decomposition, leading to deterioration of the material shown in the equation I.



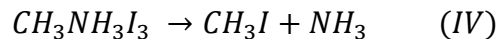
When exposed to thermal stress, CH₃NH₃PbI₃ degrades rapidly. At 40 C it first degrades and produces PbI₂ which again decomposes to lead oxide given in the equation II and III.

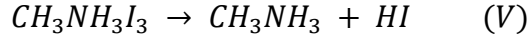
At 40 °C:



At 80 °C:

At an elevated temperature, it degrades and form CH₃NH₃I which again disintegrates to form Hydrogen Iodide shown in equation IV and V.





An alternative option to replace the toxic metal lead in perovskite materials is tin (Sn), which belongs to the same group (group 14) as lead in the periodic table. Both p-type (MASnI₃) and n-type (FASnI₃) perovskites can be obtained using tin. However, Sn-based perovskites are sensitive to air exposure. Tin exists in both 2+ and 4+ oxidation states but tends to oxidize into the Sn⁴⁺ state in ambient atmosphere. Among them, FASnI₃ is considered more stable compared to MASnI₃. All inorganic CsSnX₃ perovskites are also viable for solar cell applications. The power conversion efficiencies of CsSnI₃, CsSnBr₃, and CsSnCl₃ halides are reported to be 12.96%, 10.46%, and 9.66%, respectively [11].

Despite the potential of tin-based perovskites, it is crucial to consider that tin also has some toxic effects. Tin is classified as a carcinogen and can cause neurotoxicity. Furthermore, due to the less stable nature of Sn in perovskite materials, they may easily release hydrogen iodide (HI), leading to acidification.

Even though Sn based perovskites are not toxic as compared to Pb based Perovskites, but PCE and stability has still been a problem. Pb free cells such as FASnX₃ and CsSnX₃ are no doubt promising candidates in this regard, but they showed poor stability and power conversion efficiency as compared to lead based cells [12].

Keeping in view of this the best approach is to fabricate mixed cation cells that can solve the problem of stability as well as PCE.

2.4. Mixed Cation Perovskites:

In the perovskite structure ABX₃, A site cations holds an important position and is present at the corner positions of the crystal lattice. It plays a vital role in determining the optoelectrical properties and stability of the cell. To function as an effective light absorber, the A site cation maintains the charge neutrality along with the B site cation. Another important role is bandgap tuning, different A site cations can be employed to achieve desired bandgap. Moreover, the crystal structure, layers interface and charge transport are also influenced by the type of A site cation.

2.4.1. K-doped MAPbI3:

Research investigations conducted by Chang et al., have demonstrated that the collaborative impact of minute quantities of K⁺ can initiate the nucleation of perovskite crystals and influence their growth or the development of grain boundaries. In recent studies, researchers have introduced smaller alkali cations like K⁺ into MAPbI3 or MAFAPbI3 perovskite structures. Jung et al. observed that the lattice interplanar spacing increased following K⁺ doping, and it was noted that the steric radius of K⁺ was significantly smaller than that of CH3NH3⁺ (with K⁺ having a radius of 0.138 nm and CH3NH3⁺ having a radius of 0.203 nm).[10]

Table 2.1: Potassium halide doped Perovskite Solar cells over the years.

Perovskite (Additive)	Property	PCE % (control)	PCE % (Best)	Jsc (mA/cm ²)	Voc (V)	FF (%)	Ref.
MAPbI3 (KI)	Improving the charge carrier lifetime	13.7	15.31	20.95	0.94	79	2016 [13]
MAPbI3 (KCl)	Improving the crystallinity	11.40	15.08	19.42	1.04	74.67	2016 [14]
MAPbI3 (KI)	Improving the grain size	15.56	17.81	20.88	1.10	78	2017 [15]
FA0.85M A0.15 PbBr0.45I 2.55 (KI)	Minimizing the electron transfer barrier	18.45	20.32	22.99	1.167	76	2017 [16]

MAPbI3 (KI)	Improving carrier separation properties	17.30	19.27	23.33	1.111	74	2017 [17]
CsPbI2Br (KI)	Facilitating photoexcited charge carrier formation and transportation	8.2	10.0	11.6	1.18	73	2017 [18]
(FA0.85M A0.15)0.95 Pb(I0.85B r0.15)3 (KI)	Reduced carrier recombination	18.94	20.56	22.95	1.132	79	2017 [19]
Cs0.11MA 0.15FA0.7 4 PbI3 (KI)	Suppressing ion migration	17.3	21.5	23.2	1.17	79	2018 [20]
FA0.85M A0.15PbB r0.45 I2.55 (KI)	Decreasing defects	17.60	20.55	22.92	1.154	77.7	2018 [21]
(Cs0.06M A0.15FA0. 79) Pb(I0.85B r0.15)3 (KI)	Potassium passivation	18.2	21.6	23.06	1.18	79	2018 [22]

FA0.85M							
A0.15PbB	Preventing	17.14	17.55	21.47	1.128	72.5	2018[
r0.45	Frenkel defect						23]
I2.55 (KI)	formation						
MAPbI3—							
xClx (KCl)	Active	18.12	19.44	21.82	1.124	79.3	2018
	passivation						[24]
MAPbI3		12.73	16.59				
(KSCN)				20.45	1.065	76.20	2018
							[25]
FA0.83M	Passivating	17.1	20.4	23.5	1.15	75	2019
A0.17Pb	the grain						[26]
(I0.83Br0.	boundaries						
17)3 (KI)							

Segawa et al. conducted an evaluation of carrier lifetime and defect density, and their findings showed that K⁺ doping resulted in the lowest number of defects among the alkali cation dopants, followed by Rb⁺, Cs⁺, and Na⁺ doping in descending order. The inclusion of alkali cations can also influence the electronic characteristics of perovskite films. Jung et al. observed a substantial enhancement in crystallinity, a red shift in the photoluminescence spectrum, and a decrease in surface potential in perovskite films when doped with K⁺. This led to a noteworthy improvement in carrier separation and a reduction in charge recombination. Moreover, the introduction of K⁺ ions resulted in an extended carrier lifetime in perovskite solar cells (PSCs).[27][28]

According to Segawa et al., the incorporation of K⁺ in the perovskite layer causes the grains to become more compact, leading to larger grain sizes. Additionally, the presence of K⁺ was found to have a notable impact on the horizontal grain boundary in the perovskite structure. [9], [10]

It has been reported that the of alkali metal cations incorporation into perovskite films results in an increased grain size and a reduction in trap state density, crucial for efficient carrier transport and collection. Abdi-Jalebi et al. utilized K^+ doping to suppress halide migration and observed that perovskite films with K^+ exhibited a high and stable photoluminescence quantum efficiency (PLQE) value under continuous illumination. In contrast, pristine films experienced a gradual increase in PLQE over time due to photoinduced halide migration. The addition of K^+ is suggested to fix the excess halides by forming compounds at the grain boundaries while compensating for halide vacancies with excess iodide from potassium iodide. As a result, halide migration and light-induced ion segregation were mitigated. Confocal photoluminescence intensity maps of perovskite films with varying K^+ doping ($x = 0-0.4$) demonstrated a continuous increase in absolute emission intensity with higher K^+ content. [29] Table 2.1 shows the research work done by incorporating K into the perovskite solar cells from 2016 to 2019. The microscale photoluminescence (PL) displayed a red shift after the introduction of potassium, which aligns with absorption and electroluminescence data. Relevant PL decay curves were also reported by Segawa et al. [27]

In research conducted by Muzammal et al., K doping in $K_x(MA)_{1-x}PbI_3$ ($x=0, 0.1, 0.2, 0.3, 0.4, 1$) has reported the crystal structure change from tetragonal $MAPbI_3$ to orthorhombic $KPbI_3$ structure. It has also been observed that grain boundaries have reduced with the increased potassium doping resulting in improved morphology. Bandgap remains constant up to 50% of Potassium doping and then changes significantly to 2.6 eV upon complete doping. The findings indicate that partially doped K materials, such as $K_x(MA)_{1-x}PbI_3$ ($x=0.1, 0.2, 0.3, 0.4, 0.5$), exhibit improved crystallinity, reduced resistance, increased light absorption, enhanced stability, and optimal bandgaps, making them promising candidates for solar cell applications.[30]

2.4.2 Sn doped $MAPbI_3$:

Mixed Pb-Sn perovskite has recently gained much attention due to desirable bandgap tuning up to 1.25 eV. Keeping in view the toxicity of Pb, it contains around 50 to 60% less lead content. Apart from this, obstacles like the quick oxidation of Sn, poor career lifetime,

high defect concentration and lack of homogeneity in film morphology has been reported. [31]

Initially reported, Sn-Pb mixed perovskite solar cells (PSCs) exhibited an efficiency of approximately 25% compared to lead based perovskite solar cells. Since 2019, a lot of work has been reported in mixed Pb-Sn perovskites and the efficiency reaching 80-90% of the efficiency of Pb-based PSCs. In the latest developments, Sn-Pb mixed PSCs have achieved an impressive efficiency of 23.6%, surpassing Pb-based PSCs by 90% in terms of efficiency.[32]

Sn being the member of group 14 same as of Pb, is suitable for partial replacement of Pb for lowering the bandgap values. Sn has two oxidation states that are +2 and +4. In ambient environment Sn+2 readily oxidizes to Sn+4 which pose a challenge for device fabrication and stability. Research conducted by Ogomi et al., proved Sn as a potential candidate for effective light absorption material. They achieved a relative efficiency of 4.18% by doping 50% Sn along with Pb.[33] Main hurdle with the use of Sn as a substitute for Pb is the incorporation of Sn+2 in the crystal lattice which in turn decreases the light absorption coefficient.[34] Another issue with the use of Sn is the difference in the crystallization kinetics of Pb and Sn which affects the crystallinity and film uniformity. To address this issue, different additives have been reported in the literature like chlorides and GASCN. Prof. Yan's group reported the use of FASnI₃ along with the conventional MAPbI₃ and the resultant layer has more uniformed grains without pinholes and smaller grain size. The efficiency achieved by the inverted planar structure was reported to be 15.08% . [35]

Sn vacancies created in the lattice by the Sn+2 oxidation is another major problem resulting in low current density. The first effective additive was used by Mathews et al., by using SnF₂ as additive in PSC resulting in lower Sn vacancies. After that SnF₂ has been abundantly used additive in Sn-Pb perovskite to suppress the Sn vacancies in the crystal lattice. Kanatzidis et al., employed the use of SnF₂ in MASnI₃ and observed a reduced concentration of defects and enhanced diffusion length and carrier lifetime in the crystal lattice. [36]

In 2021, Chen et al., reported PCE of 20.27% by incorporating SnF₂ in low bandgap (FASnI₃)_{0.6}(MAPbI₃)_{0.4} perovskite solar cells. They deeply investigated the role of SnF₂

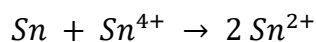
and F⁻ accumulation in the hole transport medium. Kapil et al., reported the PCE of 21.39 in Sn-Pb PCS by incorporating a different hole transport medium.[37][38] Another research carried out by Shuaifeng et al., in 2022 reported a remarkable increase in PCE. Surface modification of mixed tin-lead perovskite solar cells using ethylenediammonium diiodide and glycine hydrochloride improves carrier extraction. This treatment reduces trap densities, enhances film crystallinity, and forms surface dipoles at the charge collection interfaces, facilitating efficient charge extraction. As a result, the modified solar cells demonstrate superior performance with a fill factor of 0.82 and an impressive power conversion efficiency of up to 23.6%. [39][40]

Sn-Pb mixed perovskite materials have been relatively less explored compared to pure Pb-based perovskites. Nonetheless, systematic research has yielded remarkable progress, resulting in excellent solar cell performances. These mixed perovskites offer promising new avenues for perovskite-based materials beyond the conventional Pb-based counterparts.

2.5. Use of Sn-powder as an additive:

SnF₂ has been a proven additive for reducing Sn vacancies, but it poses limited antioxidant capacity. Tan et al., in 2019 demonstrated the limited antioxidant capability of SnF₂ by changing the color of the precursor solution from yellow to red when exposed to air. However, the use of Metallic Sn was employed, and the precursor remained stable upon exposing to air. [41][42]

The addition of Sn-powder can be better explained by comproportionation reaction. The reaction involves the formation of single intermediate oxidation state from two different oxidation states as in the reaction below:



In this reduction-oxidation reaction the Sn-powder added reduces the Sn⁺⁴ in the precursor in to 2Sn⁺². Thus, even after exposure to air the red precursor solution changes to yellow or bright yellow again. The redox reaction plays an important role in the reduction of Sn vacancies in the lattice. [43][44]

2.6. Delayed annealing of Thin Film:

A critical stage in producing perovskite thin films for solar cell applications is delayed annealing, also known as post-annealing or two-step annealing. After the first deposition and precursor treatment, a second annealing procedure is applied to the perovskite layer.

The purpose of delayed annealing in perovskite thin films is to increase the photovoltaic performance by increasing the photovoltaic efficiency, reducing the amount of defects, and improving optoelectronic characteristics. The perovskite crystals may grow and rearrange in a more regulated and stable way because to the delayed annealing process, which produces superior structural and morphological properties. Higher power conversion efficiencies result from increased charge transport and collection inside the solar cell device, which is made possible by the decreased flaws and improved crystal structure. For perovskite films based on mixed cation formulations, such as FA (Formamidinium) and MA (methylammonium) lead halides, delayed annealing has been shown to be particularly successful. Compared to their single cation counterparts, these mixed cation perovskite films frequently have better photovoltaic characteristics. Stable nanostructured inorganic-organic hybrid solar cells.

Jain et al., in 2019 demonstrated the effects of delayed annealing by a delay of 1h. The resulting film is hysteresis free and achieved a record power conversion efficiency of 16.18 %. Whereas the perovskite films deposited without this process showed only 12.35%. [45] The enhanced performance achieved by preheating treatment and delayed annealing of perovskite films can be attributed to the promotion of homogeneous nucleation and the formation of high-quality perovskite films. The improved quality of the perovskite films is evident through enhanced optoelectronic and crystalline properties of the perovskite absorber.[46]

2.7. Research gap and Proposed Solution:

From the literature it is evident that Pb free devices are not efficient in performance and lead toxicity is itself a huge environmental problem. So, the future of perovskite lies in mixed cations-based devices. Research has been conducted by doping different alkali metals into the crystal lattice of traditional MAPbI₃ devices as well as incorporating Sn at the B site.

Different agents such as SnF₂, caffeine, guanidinium thiocyanate (GuSCN) and different polymer and zwitterionic agents have been employed to control the oxidation of Sn in the structure. Research studies regarding the doping of potassium metal at the A site and partial replacement of Tin at the B site is not found. In this work, we have proposed to tune the bandgap and study the morphological structure of perovskite film by doping K and Sn at A and B site in ambient environment.

References

- [1] B. Aïssa, A. Ali, and F. El-Mellouhi, “Oxide and organic–inorganic halide perovskites with plasmonics for optoelectronic and energy applications: A contributive review,” *Catalysts*, vol. 11, no. 9, Sep. 2021, doi: 10.3390/CATAL11091057.
- [2] H. He, Z. Yang, Y. Xu, A. T. Smith, G. Yang, and L. Sun, “Perovskite oxides as transparent semiconductors: a review,” *Nano Converg*, vol. 7, no. 1, pp. 1–10, Dec. 2020, doi: 10.1186/S40580-020-00242-7/FIGURES/4.
- [3] Z. Fan, K. Sun, and J. Wang, “Perovskites for photovoltaics: a combined review of organic–inorganic halide perovskites and ferroelectric oxide perovskites,” *J Mater Chem A Mater*, vol. 3, no. 37, pp. 18809–18828, Sep. 2015, doi: 10.1039/C5TA04235F.
- [4] D. Fu, M. Itoh, D. Fu, and M. Itoh, “Ferroelectricity in Silver Perovskite Oxides,” *Ferroelectrics - Material Aspects*, Aug. 2011, doi: 10.5772/17261.
- [5] S. C. Tidrow, “Mapping Comparison of Goldschmidt’s Tolerance Factor with Perovskite Structural Conditions,” <https://doi.org/10.1080/00150193.2014.922372>, vol. 470, no. 1, pp. 13–27, Oct. 2014, doi: 10.1080/00150193.2014.922372.
- [6] A. Poglitsch and D. Weber, “Dynamic disorder in methylammoniumtrihalogenoplumbates (II) observed by millimeter-wave spectroscopy,” *J Chem Phys*, vol. 87, no. 11, pp. 6373–6378, Dec. 1987, doi: 10.1063/1.453467.
- [7] C. V. M. Vijila, A. Antony, and M. K. Jayaraj, “Perovskite Solar Cells: Concepts and Prospects,” pp. 97–133, 2022, doi: 10.1007/978-981-19-4526-7_3.
- [8] “AIST: Research Center for Photovoltaic Technologies - Functional Thin Films Team.” https://unit.aist.go.jp/rcpv/cie/r_teams/eFTFT/index.html (accessed Jul. 19, 2023).
- [9] J. Chang et al., “Enhancing the photovoltaic performance of planar heterojunction perovskite solar cells by doping the perovskite layer with alkali metal ions,” *J Mater Chem A Mater*, vol. 4, no. 42, pp. 16546–16552, Oct. 2016, doi: 10.1039/C6TA06851K.

- [10] P. Zhao et al., “Improved carriers injection capacity in perovskite solar cells by introducing A-site interstitial defects,” *J Mater Chem A Mater*, vol. 5, no. 17, pp. 7905–7911, May 2017, doi: 10.1039/C7TA01203A.
- [11] C. T. Crespo, “Contributions to Optical Properties and Efficiencies of Methyl-Ammonium Lead, Tin, and Germanium Iodide Perovskites,” *Journal of Physical Chemistry C*, vol. 124, no. 23, pp. 12305–12310, Jun. 2020, doi: 10.1021/ACS.JPCC.0C02836/ASSET/IMAGES/MEDIUM/JP0C02836_0006.GIF.
- [12] G. E. Eperon, S. D. Stranks, C. Menelaou, M. B. Johnston, L. M. Herz, and H. J. Snaith, “Formamidinium lead trihalide: A broadly tunable perovskite for efficient planar heterojunction solar cells,” *Energy Environ Sci*, vol. 7, no. 3, pp. 982–988, Mar. 2014, doi: 10.1039/C3EE43822H.
- [13] J. Chang et al., “Enhancing the photovoltaic performance of planar heterojunction perovskite solar cells by doping the perovskite layer with alkali metal ions,” *J Mater Chem A Mater*, vol. 4, no. 42, pp. 16546–16552, Oct. 2016, doi: 10.1039/C6TA06851K.
- [14] K. M. Boopathi et al., “Synergistic improvements in stability and performance of lead iodide perovskite solar cells incorporating salt additives,” *J Mater Chem A Mater*, vol. 4, no. 5, pp. 1591–1597, Jan. 2016, doi: 10.1039/C5TA10288J.
- [15] W. Zhao, Z. Yao, F. Yu, D. Yang, and S. F. Liu, “Alkali Metal Doping for Improved CH₃NH₃PbI₃ Perovskite Solar Cells,” *Advanced Science*, vol. 5, no. 2, Feb. 2018, doi: 10.1002/ADVS.201700131.
- [16] Z. Tang et al., “Hysteresis-free perovskite solar cells made of potassium-doped organometal halide perovskite,” *Sci Rep*, vol. 7, no. 1, pp. 12183–12183, Sep. 2017, doi: 10.1038/S41598-017-12436-X.
- [17] P. Zhao et al., “Improved carriers injection capacity in perovskite solar cells by introducing A-site interstitial defects,” *J Mater Chem A Mater*, vol. 5, no. 17, pp. 7905–7911, May 2017, doi: 10.1039/C7TA01203A.

- [18] J. K. Nam et al., “Potassium Incorporation for Enhanced Performance and Stability of Fully Inorganic Cesium Lead Halide Perovskite Solar Cells,” *Nano Lett*, vol. 17, no. 3, pp. 2028–2033, Mar. 2017, doi: 10.1021/ACS.NANOLETT.7B00050.
- [19] T. Bu et al., “A novel quadruple-cation absorber for universal hysteresis elimination for high efficiency and stable perovskite solar cells,” *Energy Environ Sci*, vol. 10, no. 12, pp. 2509–2515, Dec. 2017, doi: 10.1039/C7EE02634J.
- [20] M. Abdi-Jalebi et al., “Maximizing and stabilizing luminescence from halide perovskites with potassium passivation,” *Nature*, vol. 555, no. 7697, pp. 497–501, Mar. 2018, doi: 10.1038/NATURE25989.
- [21] Z. Tang et al., “Modulations of various alkali metal cations on organometal halide perovskites and their influence on photovoltaic performance,” *Nano Energy*, vol. 45, pp. 184–192, Mar. 2018, doi: 10.1016/J.NANOEN.2017.12.047.
- [22] M. Abdi-Jalebi et al., “Potassium-and rubidium-passivated alloyed perovskite films: Optoelectronic properties and moisture stability,” *ACS Energy Lett*, vol. 3, no. 11, pp. 2671–2678, Nov. 2018, doi: 10.1021/ACSENERGYLETT.8B01504/ASSET/IMAGES/LARGE/NZ-2018-01504R_0005.JPEG.
- [23] D. Y. Son et al., “Universal Approach toward Hysteresis-Free Perovskite Solar Cell via Defect Engineering,” *J Am Chem Soc*, vol. 140, no. 4, pp. 1358–1364, Jan. 2018, doi: 10.1021/JACS.7B10430/SUPPL_FILE/JA7B10430_SI_001.PDF.
- [24] P. Wang et al., “Boosting the performance of perovskite solar cells through a novel active passivation method,” *J Mater Chem A Mater*, vol. 6, no. 32, pp. 15853–15858, Aug. 2018, doi: 10.1039/C8TA05593A.
- [25] Y. Chen, J. Yang, S. Wang, Y. Wu, N. Yuan, and W. H. Zhang, “Interfacial Contact Passivation for Efficient and Stable Cesium-Formamidinium Double-Cation Lead Halide Perovskite Solar Cells,” *iScience*, vol. 23, no. 1, p. 100762, Jan. 2020, doi: 10.1016/J.ISCI.2019.100762.

- [26] P. Hang et al., “An Interlayer with Strong Pb-Cl Bond Delivers Ultraviolet-Filter-Free, Efficient, and Photostable Perovskite Solar Cells,” *iScience*, vol. 21, p. 217, Nov. 2019, doi: 10.1016/J.ISCI.2019.10.021.
- [27] S. D. Stranks, R. L. Z. Hoye, D. Di, R. H. Friend, and F. Deschler, “The Physics of Light Emission in Halide Perovskite Devices.,” *Adv Mater*, vol. 31, no. 47, pp. e1803336–e1803336, Sep. 2018, doi: 10.1002/ADMA.201803336.
- [28] X.-Y. Zhu et al., “Improved photovoltaic properties of nominal composition $\text{CH}_3\text{NH}_3\text{Pb}_{0.99}\text{Zn}_{0.01}\text{I}_3$ carbon-based perovskite solar cells,” *Optics Express*, Vol. 26, Issue 26, pp. A984–A995, vol. 26, no. 26, pp. A984–A995, Dec. 2018, doi: 10.1364/OE.26.00A984.
- [29] M. Abdi-Jalebi et al., “Maximizing and stabilizing luminescence from halide perovskites with potassium passivation,” *Nature*, vol. 555, no. 7697, pp. 497–501, Mar. 2018, doi: 10.1038/nature25989.
- [30] M. Muzammal uz Zaman et al., “Potassium doped methylammonium lead iodide (MAPbI_3) thin films as a potential absorber for perovskite solar cells; structural, morphological, electronic and optoelectric properties,” *Physica B Condens Matter*, vol. 522, pp. 57–65, Oct. 2017, doi: 10.1016/J.PHYSB.2017.07.067.
- [31] T. H. Han, S. Tan, J. Xue, L. Meng, J. W. Lee, and Y. Yang, “Interface and Defect Engineering for Metal Halide Perovskite Optoelectronic Devices,” *Advanced Materials*, vol. 31, no. 47, Nov. 2019, doi: 10.1002/adma.201803515.
- [32] J. Sun, J. Wu, X. Tong, F. Lin, Y. Wang, and Z. M. Wang, “Organic/Inorganic Metal Halide Perovskite Optoelectronic Devices beyond Solar Cells.,” *Adv Sci (Weinh)*, vol. 5, no. 5, p. 1700780, May 2018, doi: 10.1002/advs.201700780.
- [33] Y. Ogomi et al., “ $\text{CH}_3\text{NH}_3\text{Sn}_x\text{Pb}_{(1-x)}\text{I}_3$ perovskite solar cells covering up to 1060 nm,” *Journal of Physical Chemistry Letters*, vol. 5, no. 6, pp. 1004–1011, Mar. 2014, doi: 10.1021/JZ5002117/SUPPL_FILE/JZ5002117_SI_001.PDF.

- [34] J. Tong et al., “Carrier lifetimes of >1 ms in Sn-Pb perovskites enable efficient all-perovskite tandem solar cells,” *Science* (1979), vol. 364, no. 6439, pp. 475–479, 2019, doi: 10.1126/science.aav7911.
- [35] T. Jiang and Y. M. Yang, “Efficiency breakthrough for all-perovskite tandem solar cells,” *Sci China Chem*, vol. 63, no. 3, pp. 294–295, Mar. 2020, doi: 10.1007/S11426-019-9651-0/METRICS.
- [36] F. Hao, C. C. Stoumpos, R. P. H. Chang, and M. G. Kanatzidis, “Anomalous band gap behavior in mixed Sn and Pb perovskites enables broadening of absorption spectrum in solar cells,” *J Am Chem Soc*, vol. 136, no. 22, pp. 8094–8099, Jun. 2014, doi: 10.1021/JA5033259.
- [37] Q. Chen et al., “Unveiling roles of tin fluoride additives in high-efficiency low-bandgap mixed tin-lead perovskite solar cells,” *Adv Energy Mater*, vol. 11, no. 29, p. 2101045 (10 pp.), Aug. 2021, doi: 10.1002/AENM.202101045.
- [38] “G.M. Lin, Y.W. Lin, H. Huang, R.L. Cui, X.H. Guo, B. Liu, J.Q. Dong, X.F. Guo, B.Y. Sun, *Nano Energy* 27, 638 (2016) - Google Search.” https://www.google.com/search?q=G.M.+Lin%2C+Y.W.+Lin%2C+H.+Huang%2C+R.L.+Cui%2C+X.H.+Guo%2C+B.+Liu%2C+J.Q.+Dong%2C+X.F.+Guo%2C+%0D%0AB.Y.+Sun%2C+Nano+Energy+27%2C+638+%282016%29&client=firefox-b-d&sxsrf=AB5stBgkj7MerfMp8XuUtXowGOnMPk4UDw%3A1689596267361&ei=azG1ZLytFeOqkdUPvfax-AU&ved=0ahUKEwj8jtHK3JWAAxVjVaQEHT17DF8Q4dUDCA4&uact=5&oq=G.M.+Lin%2C+Y.W.+Lin%2C+H.+Huang%2C+R.L.+Cui%2C+X.H.+Guo%2C+B.+Liu%2C+J.Q.+Dong%2C+X.F.+Guo%2C+%0D%0AB.Y.+Sun%2C+Nano+Energy+27%2C+638+%282016%29&gs_l=EGxnd3Mtd2l6LXNlcnAidEcuTS4gTGluLCBZLlcuIExpbiwgSC4gSHVhbmcsIFluTC4gQ3VpLCBYLkguIEd1bywgQi4gTGl1LCBKLlEuIERvbmcsIFguRi4gR3VvLCAKQi5ZLiBTdW4sIE5hbm8gRW5lcmd5IDI3LCA2MzggKDIwMTYpSABQAFgAcAB4AZABAJgBAKABAKoBALgBA8gBAPgBAvgBAeIDBBgAIEE&sclient=gws-wiz-serp (accessed Jul. 17, 2023).

- [39] S. Hu et al., “Optimized carrier extraction at interfaces for 23.6% efficient tin–lead perovskite solar cells,” *Energy Environ Sci*, vol. 15, no. 5, pp. 2096–2107, May 2022, doi: 10.1039/D2EE00288D.
- [40] H. Lee, S. B. Kang, S. Lee, K. Zhu, and D. H. Kim, “Progress and outlook of Sn–Pb mixed perovskite solar cells,” *Nano Converg*, vol. 10, no. 1, Dec. 2023, doi: 10.1186/S40580-023-00371-9.
- [41] R. Lin et al., “Monolithic all-perovskite tandem solar cells with 24.8% efficiency exploiting comproportionation to suppress Sn(ii) oxidation in precursor ink,” *Nature Energy* 2019 4:10, vol. 4, no. 10, pp. 864–873, Sep. 2019, doi: 10.1038/s41560-019-0466-3.
- [42] T. Wu et al., “Efficient and stable tin-based perovskite solar cells by introducing π -conjugated Lewis base,” *Sci China Chem*, vol. 63, no. 1, pp. 107–115, Jan. 2020, doi: 10.1007/S11426-019-9653-8/METRICS.
- [43] H. Lee, S. B. Kang, S. Lee, K. Zhu, and D. H. Kim, “Progress and outlook of Sn–Pb mixed perovskite solar cells,” *Nano Converg*, vol. 10, no. 1, Dec. 2023, doi: 10.1186/S40580-023-00371-9.
- [44] Q. Chen et al., “Controllable self-induced passivation of hybrid lead iodide perovskites toward high performance solar cells,” *Nano Lett*, vol. 14, no. 7, pp. 4158–4163, Jul. 2014, doi: 10.1021/NL501838Y.
- [45] H. Liu, H. Liu, J. Yang, F. Yang, Z. Liu, and S. M. Jain, “Improving the Performance of Planar Perovskite Solar Cells through a Preheated, Delayed Annealing Process to Control Nucleation and Phase Transition of Perovskite Films,” *Cryst Growth Des*, vol. 19, no. 8, pp. 4314–4323, Aug. 2019, doi: 10.1021/ACS.CGD.9B00024/SUPPL_FILE/CG9B00024_SI_001.PDF.
- [46] L. Zuo et al., “Enhanced photovoltaic performance of CH₃NH₃PbI₃ perovskite solar cells through interfacial engineering using self-assembling monolayer,” *J Am Chem Soc*, vol. 137, no. 7, pp. 2674–2679, Feb. 2015, doi: 10.1021/JA512518R/SUPPL_FILE/JA512518R_SI_001.PDF.

Chapter 3

Brief detail of Experimental Techniques

The chapter briefly describes the use of Laboratory equipment for deposition and characterization of thin films. Moreover, it also explains the working principle of these techniques.

3.1 Plasma Cleaning

Plasma cleaning is a method of improving the cleanliness of materials by using low-pressure plasma to remove impurities from their surfaces. The plasma creates highly reactive species when it ionizes a gas, and these species then interact with the surface being treated. Various sectors can benefit from this interaction's breakdown and removal of organic and inorganic pollutants. Additionally, surface activation by plasma cleaning improves surfaces' wettability and adhesion capabilities. It provides selectivity, enabling the targeting of pollutants or materials while sparing the surrounding environment. Because it uses fewer chemicals and produces less toxic byproducts, the process is considered environmentally friendly and non-destructive. It also operates at low temperatures. Plasma cleaning, as a whole, is a flexible method for producing clean and activated surfaces in a controlled and environmentally responsible way. [1]



Figure 0.1: Plasma Cleaner

Plasma cleaning works by generating plasma, which is made up of highly reactive species like ions, radicals, and electrons, in a low-pressure environment. This is accomplished by exposing a gas, such as oxygen or a mixture of gases, inside a vacuum chamber to an energy source, often radiofrequency power. Contaminants on the treated surface interact with the energetic plasma species. Organic compounds, inorganic residues, or oxide layers are examples of these pollutants. The pollutants and reactive species interact chemically, causing the contaminants' chemical bonds to be broken and turning them into volatile byproducts. The surface is then cleaned of the volatile byproducts. Vacuum pumping or gas flow are often used for this cleanup, which helps to remove the byproducts and prevent recontamination of the surface. In addition to cleaning, plasma treatment also activates the surface. The energetic species within the plasma can modify the surface's chemical composition and create reactive sites. This surface activation enhances the surface's adhesion properties, improving bonding capabilities and promoting better wetting of liquids on the surface. [2]

For plasma cleaning to be successful, precise control over a variety of process variables is essential. These variables include the gas composition, the pressure, the power, the duration of the treatment, and any unique factors pertaining to the substance being treated. The best cleaning results can be achieved while limiting potential surface damage by adjusting these values. In general, plasma cleaning offers a diverse and controlled process for clearing away impurities and energizing surfaces. It is a vital technology in fields where cleanliness and surface preparation are crucial because to its benefits like selectivity, non-destructiveness, and environmental friendliness.

3.2 Glove Box:

A glove box, often referred to as a glove chamber or an isolation chamber, is a closed container that offers a controlled environment for handling delicate items or carrying out experiments that demand a high level of security. It has a glass front panel and integrated gloves that let users handle the contents of the box without jeopardizing the regulated environment. A glove box's main purpose is to create a closed environment. To offer visibility while preserving a sealed environment, the enclosure is often built of a transparent material like acrylic or polycarbonate. Operators can operate items or carry out operations

within the glove box without coming into direct touch thanks to the gloves that are affixed to the front panel.

Glove boxes can be customized with a range of features to satisfy particular needs. These might include humidity and temperature controls, integrated monitoring systems to keep tabs on environmental conditions inside the box, and airlock systems for transferring samples or materials in and out of the box without compromising the controlled atmosphere. Gas purification systems may also be used to maintain an inert or particular gas environment. The ability to maintain a controlled environment devoid of moisture, oxygen, or other contaminants that could adversely affect delicate materials or experiments is one of the main benefits of employing a glove box. The glove box is completely sealed, protecting the contents' integrity and purity from the entry of outside pollutants. [3]



Figure 0.2: Glove Box

Glove boxes also provide operator protection. They put up a wall between the handler and the objects being handled, shielding them from reactions or substances that could be dangerous. Usually made of materials that are resistant to chemicals, the gloves offer a secure working environment. Glove boxes offer a safe and secure environment for working with delicate items or carrying out experiments that need to be isolated. They guarantee operator safety, provide contamination prevention, and uphold controlled environments. Glove boxes are crucial instruments in a variety of scientific and commercial settings because of their adaptability and customization choices.

3.3 Spin coater:

A spin coater is a tool used in many businesses and research settings to coat a substrate uniformly and thinly. It consists of a rotating platform on which the substrate is put, usually consisting of a flat surface or a chuck. The substrate can be a glass slide, a wafer, or any other flat surface that needs to be coated.

The spin coater works by depositing a liquid solution onto the substrate's core, such as a polymer or thin film material. Centrifugal force spreads the liquid across the substrate while the platform rotates quickly, forming a thin layer that sticks to the surface. The liquid can spread evenly and form a thin layer with controllable thickness thanks to the spinning process. To get the right coating qualities, like thickness and coverage, you can change the spin's speed and duration [4].

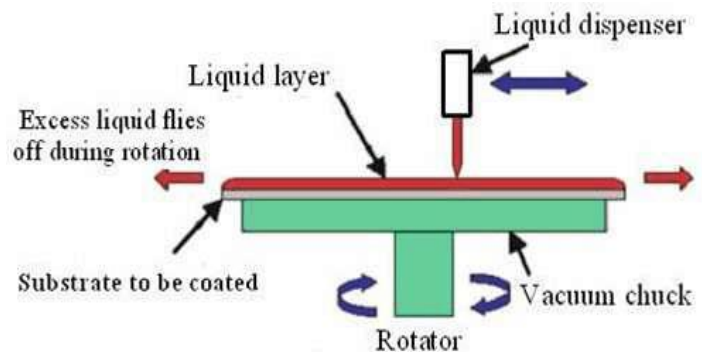


Figure 0.3: Spin Coater [5]

In processes like thin film deposition, photoresist coating in the production of semiconductors, and surface modification in materials science, spin coaters are frequently employed. They provide benefits like accurate coating parameter control, high repeatability, and quick coating deposition.

To apply the desired coating on a substrate, a spin coater goes through a sequence of processes. First, the rotating platform is properly positioned onto the substrate. The coating ingredient is then poured onto the substrate's center as a liquid solution. Centrifugal forces

spread the liquid outward when the platform begins rotating rapidly, generating a thin and uniform coating across the substrate surface. The coating material is solidified and stabilized as the spin coater spins in order to permit solvent evaporation. The coating quality is next examined to make sure the desired standards are met for uniformity and thickness. Spin coaters provide a dependable way for quick and uniform coating deposition since they allow for exact control over rotation speed, duration, and liquid dispensing. They find applications in diverse industries such as semiconductor manufacturing, optics, and materials research.

3.4 Scanning Electron Microscopy

An advanced imaging method known as scanning electron microscopy (SEM) produces three-dimensional, high-resolution images of a sample's surface. SEM picks up signals produced by the interaction of the focused electron beam and the sample by scanning it across the sample. It is possible to identify and use these signals, which include secondary electrons, backscattered electrons, and distinctive X-rays, to produce in-depth visual images. At magnifications ranging from nanometers to micrometers, SEM enables researchers to examine the topography, morphology, and composition of numerous materials. SEM is an important tool for examining and characterizing surface structures with unmatched accuracy and detail, with applications in a variety of disciplines including materials science, nanotechnology, biology, and geology.

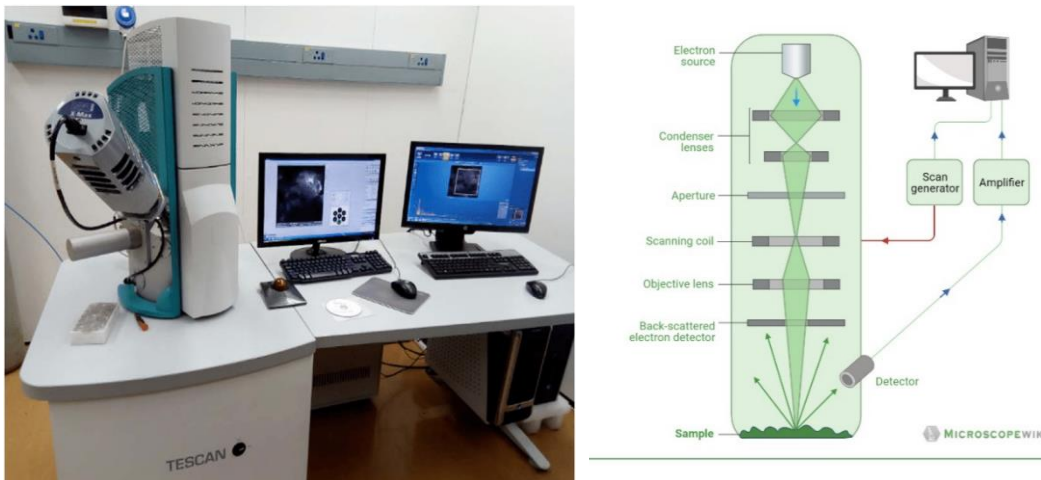


Figure 0.4: Scanning Electron Microscope [6]

By moving a concentrated electron beam across a sample's surface, scanning electron microscopy (SEM) creates signals that are detected and used to build images. When an electron beam interacts with a material, secondary electrons, backscattered electrons, and distinctive X-rays are produced. The electron beam is produced by an electron source and focussed using electromagnetic lenses. Backscattered electrons supply compositional contrast, while secondary electrons offer topographical information. Elemental analysis is possible with distinctive X-rays. These signals are gathered by detectors, analyzed, and transformed into digital data. The image exhibiting the surface topography, morphology, and composition of the sample is made using the signals that have been processed. By examining materials under high magnification and resolution with SEM, researchers can learn important details about their microstructure and composition. It finds applications in various fields, including materials science, nanotechnology, biology, and geology, where detailed surface analysis is essential [7].

3.5 X-ray Diffraction

An analytical method for examining the crystallographic characteristics of materials is X-ray diffraction (XRD). A sample is exposed to X-rays, and the sample's diffraction pattern is then examined to reveal information on the sample's crystal structure, lattice parameters, and phase composition. It is used in solid-state physics, geology, chemistry, materials science, and other fields to help researchers identify phases, figure out crystal structures, and examine structural changes brought on by outside influences. Understanding the atomic structure and characteristics of crystalline materials requires the use of X-ray diffractograms (XRD).

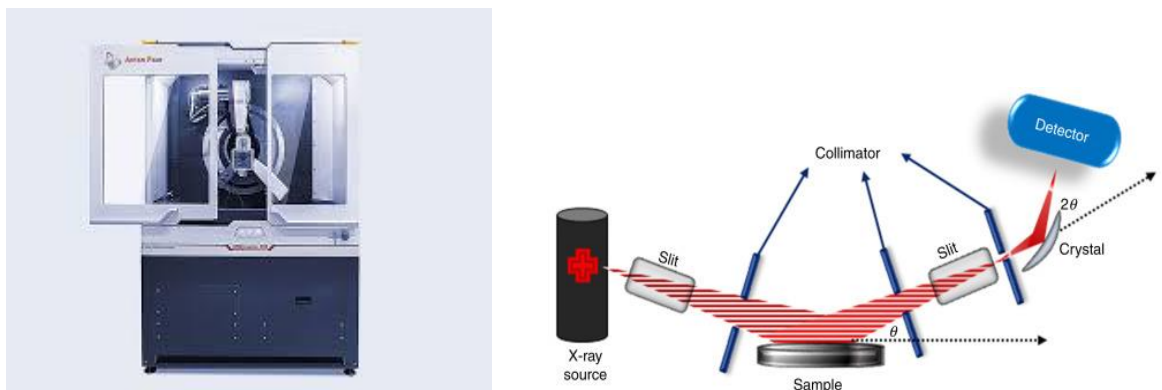


Figure 0.5: X-ray diffraction (XRD) [8]

A monochromatic X-ray beam is focused onto a crystalline sample during X-ray diffraction (XRD), which then examines the diffraction pattern. X-rays scatter and produce both constructive and destructive interference patterns when they interact with the atoms in the crystal lattice. On a detector, the dispersed X-rays produce a diffraction pattern of brilliant spots or peaks. The crystal structure, lattice parameters, and phase composition of the substance can be ascertained by rotating the sample and measuring the intensity and angle of the scattered X-rays. The diffraction pattern is compared to well-known crystal structures utilizing mathematical methods and crystallographic databases to gain this information. XRD is a non-destructive technique widely used in materials science, geology, chemistry, and solid-state physics for phase identification, determination of crystal structures, and studying structural changes induced by external factors. It provides valuable insights into the atomic arrangement and structural properties of crystalline materials [8], [9].

3.6 Fourier Transform Infrared Spectroscopy

FTIR (Fourier Transform Infrared Spectroscopy) is an analytical technique used to analyze the chemical composition of materials by measuring their interaction with infrared light. It creates a distinctive spectral fingerprint using the chemicals inside a sample's absorption at particular infrared wavelengths. The data is transformed into an infrared spectrum by applying a Fourier Transform to the interferogram produced by an interferometer. The identification and analysis of the sample are aided by the spectrum's essential information about the functional groups and chemical bonds contained in the sample. Due to its non-destructive nature and capacity to quickly determine a substance's molecular structure and composition, FTIR is often used in a variety of scientific disciplines, including materials science, medicines, forensics, and environmental monitoring.

When using FTIR (Fourier Transform Infrared Spectroscopy), a sample is exposed to a wide variety of infrared wavelengths, which interact with the molecules there. The vibrational modes of the molecules determine which infrared frequencies they absorb. An interferometer is used to analyze the light that the sample has either transmitted or reflected. An interferogram is produced by combining the sample and reference beams that the

interferometer separates into. Information regarding the sample's infrared frequency absorption is contained in the interferogram. The interferogram is transformed into a spectrum that displays the sample's infrared absorption as a function of frequency by performing a Fourier Transform. The resultant spectrum exhibits distinctive peaks and

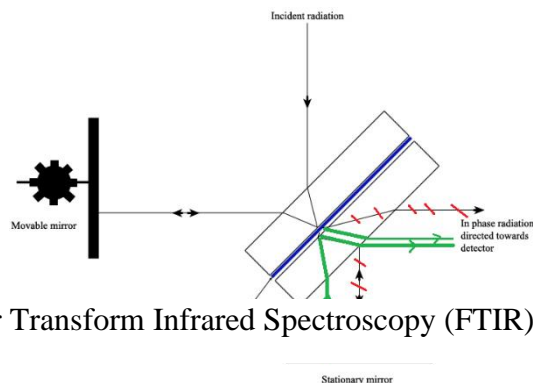


Figure 0.6: Fourier Transform Infrared Spectroscopy (FTIR) working structure [11]

patterns that line up with the functional groups and chemical bonds in the sample. By comparing the obtained spectrum to spectral databases, the chemical composition and structure of the sample can be analyzed. FTIR spectroscopy is widely used in various fields for its ability to provide insights into the molecular composition and structure of substances based on their infrared absorption properties. [10], [11]

3.7 UV-vis Spectroscopy:

UV-Vis spectroscopy is a method of analysis that assesses how well a material transmits and absorbs ultraviolet and visible light. Its foundation is the idea that molecules absorb particular light wavelengths that correspond to their electrical transitions. You may learn important details about a sample's electronic structure, concentration of absorbing species, and chemical characteristics by shining a UV or visible light through it and measuring how much light is absorbed or transmitted. Numerous disciplines, including chemistry, biochemistry, pharmacology, environmental studies, and materials research, make extensive use of UV-Vis spectroscopy. It offers a quick, easy, and flexible way for classifying and evaluating a variety of compounds based on how they interact with UV and visible light.

UV-Vis spectroscopy measures light transmission and absorption by shining a UV or visible light through a material. A wide range of wavelengths are emitted by the light

source, and as the light interacts with the sample, some of these wavelengths are absorbed by the molecules there. The remaining light passes through the sample and is detected by a photomultiplier tube or photodiode. To take into account any modifications to the spectrophotometer system or light source, a reference measurement is made. The quantity of light absorbed by the sample is calculated by comparing the reference and sample's transmitted light intensities. The spectrophotometer scans a range of wavelengths, generating an absorption spectrum that provides information about the sample's electronic structure, concentration of absorbing species, and chemical properties. UV-Vis spectroscopy

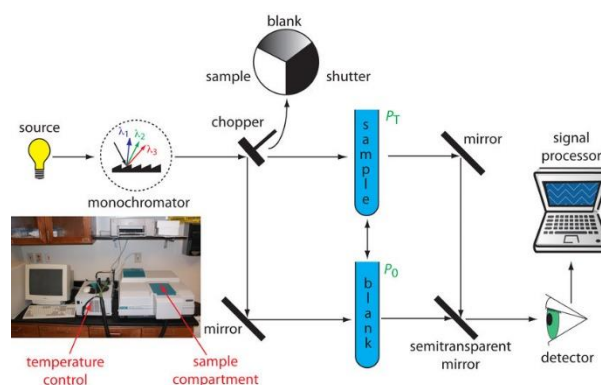


Figure 0.7: Working mechanism of UV-vis Spectroscopy [12]

is widely used in various fields for its simplicity, speed, and ability to characterize substances based on their interaction with UV and visible light. [13]

3.8 Photoluminescence

The spectroscopy method known as photoluminescence (PL) involves a substance emitting light after absorbing photons. It is possible to learn important details about the material's composition, bandgap, and defect states by examining the light that is emitted. Materials science, semiconductor research, optoelectronics, and bioimaging are just a few of the domains where PL is frequently employed since it sheds light on the electrical and optical properties of materials.

The absorption of photons by a substance, the subsequent excitation of electrons to higher energy levels, relaxation processes, and the emission of light are the components of the photoluminescence (PL) mechanism. The electrons in a material's atoms absorb the energy from photons and get excited. Known as photoluminescence, the surplus energy is

released as these excited electrons relax back into lower energy levels. Depending on the characteristics of the material, the light that is released may have a different wavelength or color from the photons that are absorbed. The electrical structure, energy levels, flaws, and composition of the material may all be learned by examining the light that is emitted. Photoluminescence spectroscopy provides insights into the optical and electronic characteristics of materials and finds applications in various fields, such as semiconductor research, materials science, optoelectronics, and bioimaging. [14]

Summary

The chapter provides a brief overview of laboratory equipment used for deposition and characterization of thin films. It discusses the working principles of several techniques, including plasma cleaning, glove boxes, spin coaters, scanning electron microscopy (SEM), X-ray diffraction (XRD), Fourier Transform Infrared Spectroscopy (FTIR), UV-Vis spectroscopy, and photoluminescence (PL). Each technique is described in terms of its working mechanism and applications. The chapter highlights how these techniques are used to achieve clean and activated surfaces, maintain controlled environments, deposit thin films, analyze surface structures, study crystallographic properties, and analyze the chemical composition of materials. It emphasizes the importance of these techniques in various scientific and industrial fields, such as materials science, semiconductor research, nanotechnology, and bioimaging.

References

- [1] D. F. O’Kane and K. L. Mittal, “Plasma cleaning of metal surfaces,” *Journal of Vacuum Science and Technology*, vol. 11, no. 3, pp. 567–569, May 1974, doi: 10.1116/1.1318069.
- [2] T. C. Isabell, P. E. Fischione, C. O’Keefe, M. U. Guruz, and V. P. Dravid, “Plasma Cleaning and Its Applications for Electron Microscopy,” *Microscopy and Microanalysis*, vol. 5, no. 2, pp. 126–135, 1999, doi: 10.1017/S1431927699000094.
- [3] J. G. Pack and G. G. Libowitz, “A Versatile, Inert Atmosphere Vacuum Glove Box,” *Review of Scientific Instruments*, vol. 40, no. 3, pp. 414–419, Mar. 1969, doi: 10.1063/1.1683961.
- [4] “Spin Coating - an overview | ScienceDirect Topics.” <https://www.sciencedirect.com/topics/materials-science/spin-coating> (accessed Jul. 19, 2023).
- [5] “Schematic of spin coating process. | Download Scientific Diagram.” https://www.researchgate.net/figure/Schematic-of-spin-coating-process_fig1_335638190 (accessed Jul. 19, 2023).
- [6] “Scanning Electron Microscope (SEM) - Diagram, Working Principle, Components and Cost.” <https://microscopewiki.com/scanning-electron-microscope/> (accessed Jul. 19, 2023).
- [7] K. Akhtar, S. A. Khan, S. B. Khan, and A. M. Asiri, “Scanning electron microscopy: Principle and applications in nanomaterials characterization,” *Handbook of Materials Characterization*, pp. 113–145, Sep. 2018, doi: 10.1007/978-3-319-92955-2_4/COVER.
- [8] “X Ray Diffraction - an overview | ScienceDirect Topics.” <https://www.sciencedirect.com/topics/nursing-and-health-professions/x-ray-diffraction> (accessed Jul. 19, 2023).
- [9] E. Donnelly and A. L. Boskey, “Mineralization,” *Vitamin D: Two-Volume Set*, vol. 1–2, pp. 381–401, Jun. 2011, doi: 10.1016/B978-0-12-381978-9.10021-6.

- [10] “FTIR: Fourier-Transform Infrared Spectroscopy Principles and Applications.” <https://www.findlight.net/blog/ftir-principles-applications/> (accessed Jul. 19, 2023).
- [11] “How an FTIR Spectrometer Operates - Chemistry LibreTexts.” https://chem.libretexts.org/Bookshelves/Physical_and_Theoretical_Chemistry_Textbook_Maps/Supplemental_Modules_%28Physical_and_Theoretical_Chemistry%29/Spectroscopy/Vibrational_Spectroscopy/Infrared_Spectroscopy/How_an_FTIR_Spectrometer_Operates (accessed Jul. 19, 2023).
- [12] “7: Mechanism of UV visible spectrometer. | Download Scientific Diagram.” https://www.researchgate.net/figure/Mechanism-of-UV-visible-spectrometer_fig7_334654292 (accessed Jul. 19, 2023).
- [13] “Ultraviolet-Visible (UV-Vis) Spectroscopy: Principle and Uses | Analytical Chemistry | JoVE.” <https://www.jove.com/v/10204/ultraviolet-visible-uv-vis-spectroscopy> (accessed Jul. 19, 2023).
- [14] “Photoluminescence - Wikipedia.” <https://en.wikipedia.org/wiki/Photoluminescence> (accessed Jul. 19, 2023).

Chapter 4

Experimental Work

This chapter briefly describes the experimental setup designed for the preparation of precursors and the equitable quantities of solutes and solvents used. Additionally, thin film deposition and the suitable external factors necessary for the deposition are also discussed.

4.1 Materials

Unless otherwise specified, all materials were utilized in their received form without any further modifications. Methylammonium Iodide (MAI) was bought from Solaronix. Lead Iodide, Tin Flouride (SnF_2) and Tin Powder were obtained from Sigma Aldrich. Potassium Iodide (KI) was purchased from Honeywell. Tin Iodide was purchased from Macklin. Anhydrous dimethyl formamide (DMF) and dimethyl Sulfoxide (DMSO) were obtained from Dukson pure Chemicals Co. Ltd.

4.2 Precursor Preparation

To study the morphological and intrinsic properties, four precursors are prepared as below:

- MAPbI_3 (as standard absorber layer)
- 40% Potassium doped MAPbI_3
- 40% Potassium doped MAPbI_3 with 10% doping of Tin.
- 40% Potassium doped MAPbI_3 with 20% doping of Tin.

a. MAPbI_3 precursor preparation

A standard amount of Methylammonium (MA) weighted 159 mg is mixed with 461mg of Lead Iodide (PbI_2). To prepare 1ml solution DMF and DMSO are added in the ration of 4:1. The solution is left overnight for stirring at a temperature of 70 C. All of this is done inside glove box.

b. 40 % Potassium doped MAPbI_3 precursor preparation

A standard amount of Methylammonium (MA) weighed 95.4 mg along with 66.4 mg of Potassium Iodide (KI) is mixed with 461mg of Lead Iodide (PbI₂). To prepare 1ml solution DMF and DMSO are added in the ration of 4:1. The solution is left overnight for stirring at a temperature of 70 C. All of this is done inside glove box.

c. 40% Potassium doped MAPbI₃ with 10 % tin doped precursor preparation

A standard amount of Methylammonium (MA) weighed 95.4 mg along with 66.4 mg of Potassium Iodide (KI) is mixed with 414.9 mg of Lead Iodide (PbI₂) and 37.2 mg Tin Iodide (SnI₂). Additionally, 15.7mg of SnF₂ is added to it. To prepare 1ml solution DMF and DMSO are added in the ration of 4:1. The solution is left overnight for stirring at a temperature of 70 C. All of this is done inside glove box. 5mg/ml of Sn- Powder is added before the deposition and then filtered.

d. 40 % Potassium doped MAPbI₃ with 20 % tin doped precursor preparation

A standard amount of Methylammonium (MA) weighed 95.4 mg along with 66.4 mg of Potassium Iodide (KI) is mixed with 368.8 mg of Lead Iodide (PbI₂) and 74.5 mg Tin Iodide (SnI₂). Additionally, 15.7mg of SnF₂ is added to it. To prepare 1ml solution DMF and DMSO are added in the ration of 4:1. The solution is left overnight for stirring at a temperature of 70 C. All of this is done inside glove box. 5mg/ml of Sn- Powder is added before the deposition and then filtered.

4.3 Deposition of Perovskite Absorber Layer

For the deposition, glass substrates were first cleaned in solution of deionized water, ethanol and Isopropanol in an ultrasonic bath for 10 minutes each. The glass substrates were then dried and undergone oxygen plasma cleaning for 10 minutes.

Each of the precursor solution is filtered with 0.22 um polytetrafluoroethylene (PTFE) filter. For the tin doped precursor Sn powder is added (5mg/ml) stirred for about 10 minutes and then filtered out. 20uL of each of the precursor is statically dropped on the substrate. In the first step the speed was 1000 rpm for 10 seconds and in the second step the speed was 4000 rpm for 30 seconds. 200 uL of Ethyl Acetate as an antisolvent was dropped in the last 15 seconds.

In the final stage, the deposited perovskite film undergone annealing in two stages. In the first stage, i.e. delayed annealing the film was annealed at room temperature for 30 minutes and then annealed at 100 C for 10 minutes on a hot plate.

4.4 Characterization Techniques used with parameters

To investigate the structural and crystallographic properties of Sn-Pb mixed perovskite films, we employed X-ray diffraction (XRD) analysis. The XRD patterns were acquired using a Bruker D8 Advanced instrument with a scan rate of 1.2/min and a 2θ range from 10° to 40° . A $\text{CuK}\alpha$ radiation source ($\lambda=1.54056 \text{ \AA}$) was utilized, with an excitation voltage of 40 kV and a current of 40 mA. The XRD data were analyzed using X'Pert HighScore Plus software. To examine the optical properties, UV-visible absorbance spectra were measured using a Shimadzu UV-3600i Plus spectrophotometer. The surface morphology of the Sn-Pb mixed perovskite absorber films was observed using a TESCAN-VEGA-3 scanning electron microscope (SEM). For EDX analysis, the same equipment was used, with the voltage set at 20 kV and a width of 15 mm. To analyze intermolecular interactions, Fourier-transform infrared spectroscopy (FTIR) was conducted using a CARY 630 FTIR instrument from Agilent Technologies, USA. The diamond attenuated total reflection (ATR) module was employed, and the wavenumber range was set from 4000 cm^{-1} to 640 cm^{-1} .

Summary:

In this chapter, experimental work has been discussed. The relative amount of each of the materials used along with the conditions in which the experiment has been performed. Moreover, the preparation of different precursors and deposition is explained. Along with that the parameters are also mentioned that are maintained while doing different characterization.

Chapter 5

Results and Discussion

5.1 Optical microscopy (OM) analysis

To understand the growth kinetics of the under-studied samples, the growth of crystals was observed by optical microscopy (OM) using a 20× magnification lens. OM images of the present MAPbI₃ doped with potassium, potassium and 10% wt. Sn, or potassium and 20% wt. Sn samples are shown in Figure 5.1(a)-(d). An image processing software (Fiji, Image J) was used to determine observable particle sizes of the samples. To compare the evolution of the crystal size, the effective radius is defined as the square root of the area $r_{eff} = \sqrt{A}$ to permit comparison directly between the complex non-spherical crystal shapes.

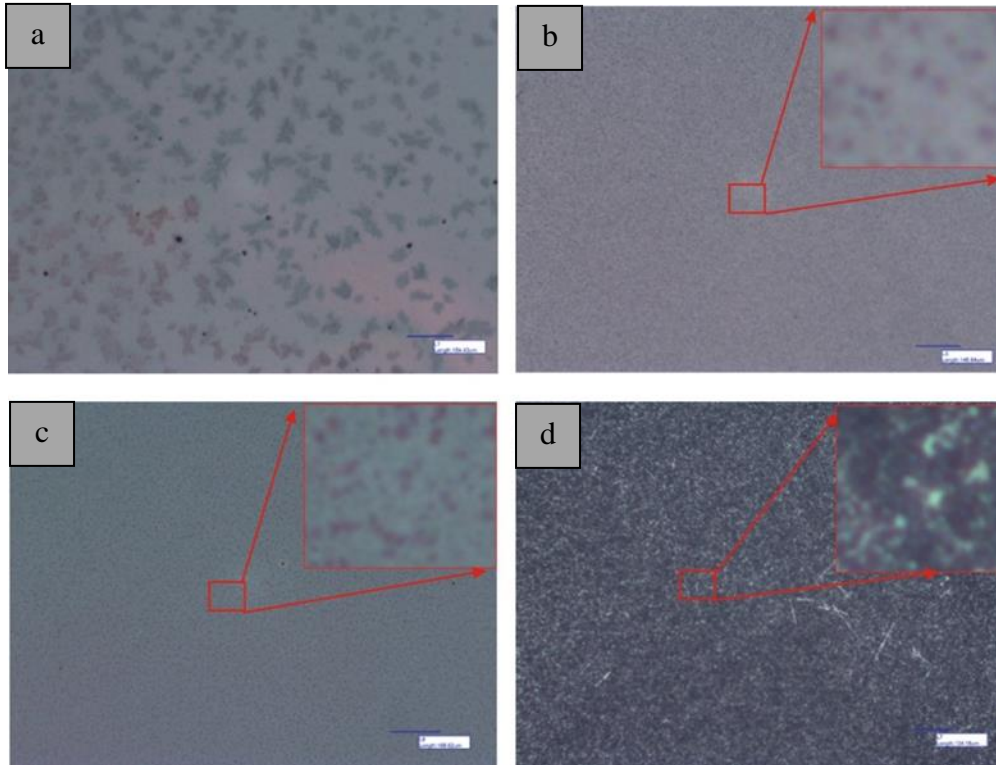


Figure 5.1: Optical microscope images of solar cells based on the following perovskite phase: (a) MAPbI₃, (b) MAPbI₃ doped with potassium, (c) MAPbI₃ doped with potassium and 10% wt. Sn, and (d) MAPbI₃ doped with potassium and 20% wt. Sn

According to Figure 5.1 (a), the growth of dendrite-like MAPbI₃ perovskite crystals, and free spaces between them is a typical morphology for the material as was seen in some other studies [1–3]. From Figure 5.1 (b)-(d), it is clear that significantly different kinetics were caused by the presence of the doped elements, which speed up the nucleation, increasing the number of crystals, affecting their morphology, and promoting heterogeneous nucleation. Edwin et al. [3] demonstrated that once r_{eff} is larger than the critical radius, individual stable nuclei continue growing. They showed for the dopant-free sample, the growth follows a reaction-limited process, whereas the films with additives follow a hindered diffusion-limited growth (presumably due to the very large number of nucleation sites). Then, those nuclei reach a maximum r_{eff} and they start forming crystals of larger length scales through aggregation. The very high nucleation rate, and therefore, overlapping of particles in the doped sample with potassium and 20% wt. Sn led to the indistinguishable particle boundaries.

In order to more accurately investigate the particle size of the under-studied samples (except for the doped sample with potassium and 20% wt. Sn due to the indistinguishable particle boundaries), 100 particles in the micrographs were measured by the above-mentioned image processing software and the histograms of particle size distribution are shown in Figure 5.2.

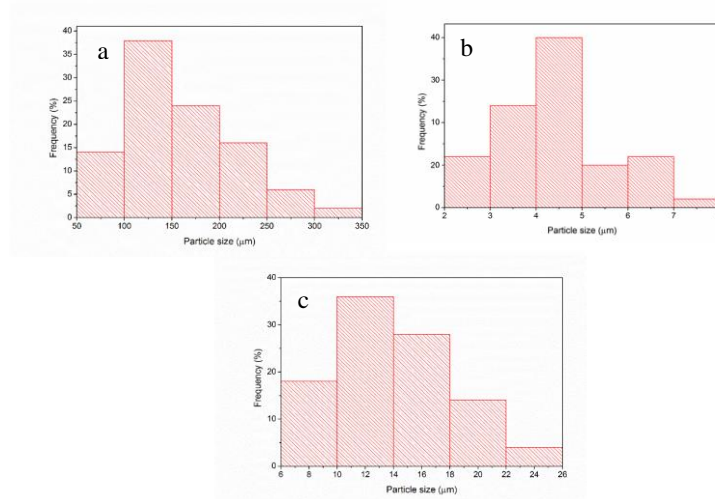


Figure 5.2: Size distribution histograms of solar cells based on the following perovskite phase: (a) MAPbI₃, (b) MAPbI₃ doped with potassium, and (c) MAPbI₃ doped with potassium and 10% wt. Sn.

In these histograms, the horizontal axis is attributed to the ranges of particle diameter sizes and the vertical axis is related to the number of particles in that size range. According to Figure 5.2 (a), in the undoped sample, among the 100 measured particles, 37 particles were in diameter size range of 100-150 μm . In the histogram of MAPbI_3 doped with potassium, 40% of the particles were in the size range of 4 to 5 μm and for the sample of MAPbI_3 doped with potassium and 10% wt. Sn, about 38% of the particles were in the size range of 10 to 14 μm . Statistical data extracted from the measurements are reported in Table 5.1.

Table 5.1: Statistical data extracted from OM micrographs

Sample	No. of measurement s	Average particle size (μm)	Standard division (μm)	Smallest particle size (μm)	Largest particle size (μm)
MAPbI_3	100	161.37	62.90	56.21	336.92
MAPbI_3 doped with potassium	100	4.41	1.19	2.39	7.91
MAPbI_3 doped with potassium and 10% wt. Sn	100	14.03	4.08	6.71	23.89

Based on Table 5.1 the significantly decrement of particle size by doping the MAPbI_3 structure is clear. However, it can be seen that the average particle size for MAPbI_3 doped with potassium and 10% wt. Sn was about 3 times more than that obtained for the sample doped with potassium. The reasons of the average particle increment in the presence of Sn element needs more investigations.

For the doped samples, it was not possible to resolve the structure in detail because of the very small features with the magnification used but only roundish crystals are observed. Therefore, scanning electron microscopy (SEM) was used to better investigate the microstructure of the under-studied samples.

5.2 SEM and EDS/Mapping analyses

Figure 5.3 (a)–(d), shows the SEM micrographs of the undoped and doped perovskite thin films on an FTO glass substrate. In addition, the results of EDS and elemental mapping analyses for the undoped and MAPbI₃ doped with potassium, potassium/10% wt. Sn, and potassium/20% wt. Sn samples are represented in Figure 5.4-5.5.

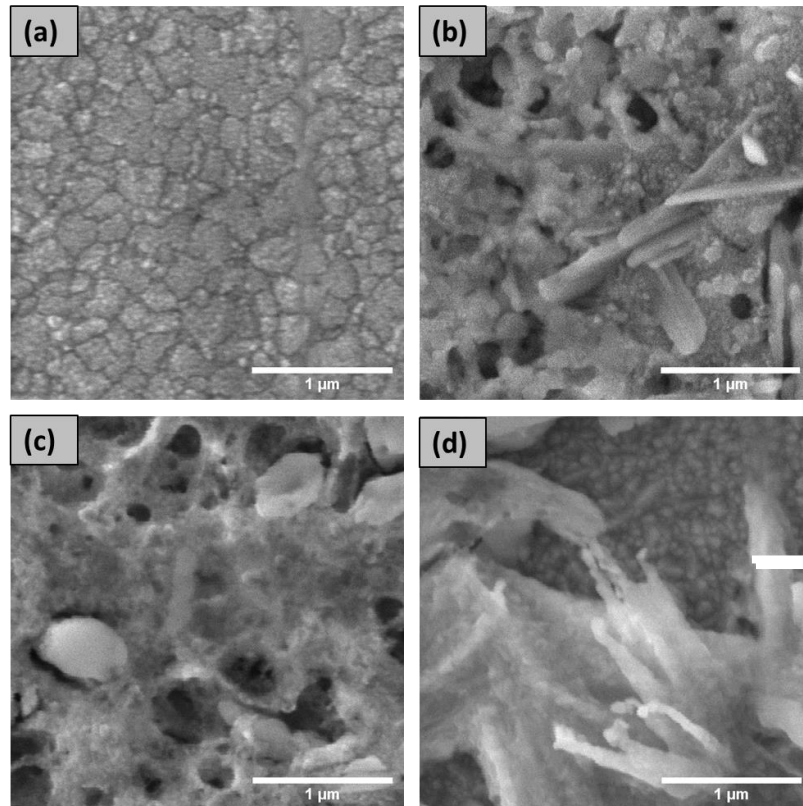


Figure 5.3: SEM micrographs of solar cells based on the following perovskite phase: (a) MAPbI₃, (b) MAPbI₃ doped with potassium, (c) MAPbI₃ doped with potassium and 10 % wt. Sn, and (d) MAPbI₃ doped with potassium and 20 % wt. Sn.

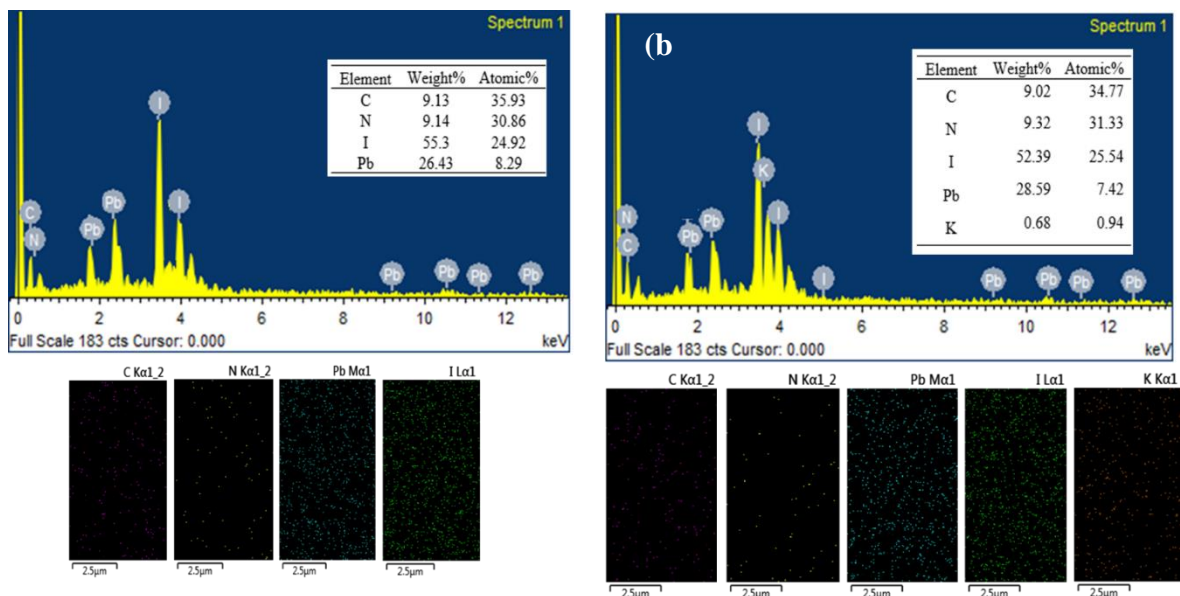


Figure 5.4: (a) EDS and elemental mapping results for the MAPbI₃ sample (b) EDS and elemental mapping results for the MAPbI₃ doped with potassium.

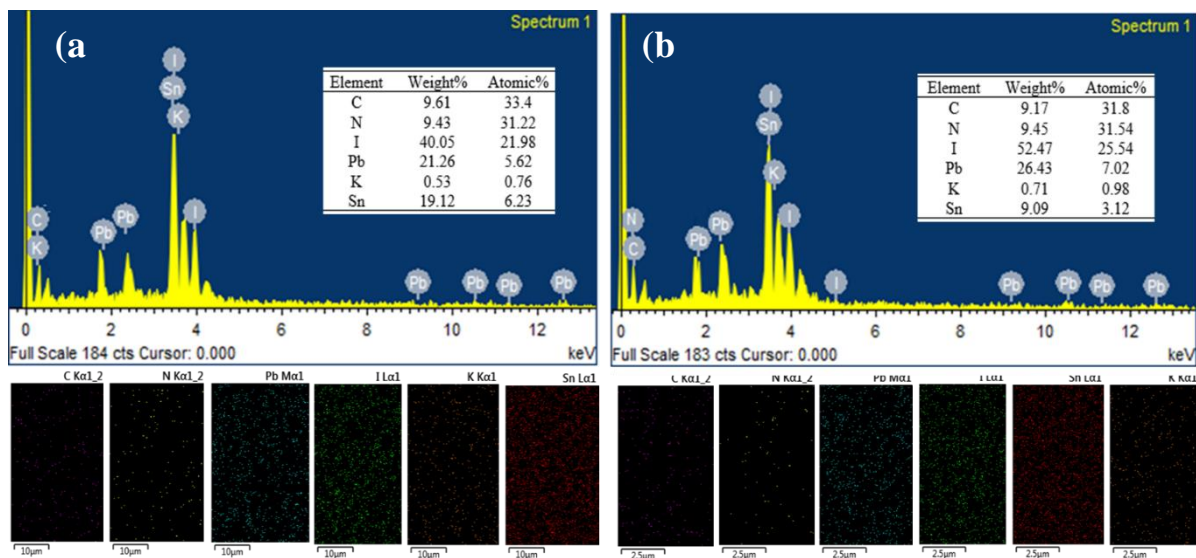


Figure 5.5: (a) EDS and elemental mapping results for the MAPbI₃ doped with potassium and 10 %wt. Sn (b) EDS and elemental mapping results for the MAPbI₃ doped with potassium and 20 %wt. Sn.

From Figure 5.3(a), the pure MAPbI₃ perovskite film exhibited compact and smooth morphologies with crystal grain sizes of 100–400 nm. Such a morphology and grain size was also observed previously for pure MAPbI₃ perovskite films formed in different conditions [4–6]. However, the surface morphologies of doped films had another vision. It can be seen that by doping of potassium element in the perovskite structure, strip-like

structures start appearing, as was seen by Zaman et al [7]. The textured film with improved voids/grain boundaries are observed with these strip like structures for the K-doped film. The gathered potassium at grain boundaries can serve as a support template and induce perovskite nucleation with lateral growth in grain boundaries because the heterogeneous nucleation can obviously lower the nucleation free-energy barrier in the grain boundaries. Thus, some small bar-shaped grains were formed in the vicinity of crystal boundaries [8]. The size of the appeared voids was in the range of 100-500 nm with an average size of about 250 nm. By introducing Sn element to the potassium doped MAPbI₃ perovskite film, the morphology was almost unchanged and only the average diameter size of the pinholes increased to about 440 nm (Figure 5.3 (c)). In addition, the surface of the Sn-K doped perovskite was rougher than the samples without Sn. However, according to Figure 5.3 (d), the perovskite film doped by potassium and 20 % wt. Sn was nearly pinhole free as compared to other potassium-containing films. Additionally, it was concluded that such doping had significant effects on the absorption and hole motilities when compared to other samples. In addition, from the Figure 5.3 (d), some relatively large clusters can be seen alongside small grains with an average particle size of around 80 nm. In fact, by further increasing the Sn concentration to 20 % wt., the abundant nucleation sites caused by Sn promote the bar-shaped particles grown up to sheet-shaped grains, which can partly remedy the exposed grain boundaries, and some bottom grains are merged into interconnected perovskite communities. The excessive nucleation sites of Sn and K along the grain boundaries are responsible for the formation of small perovskite grains, which further supports the fact that the doped elements are easily segregated in the vicinity of grain boundaries.

To determine the elemental composition of the doped and undoped samples more accurately, the EDS spectra and elemental mappings of the prepared films are shown in Figure 5.4-5.5. From Figure 5.4(a), it can be seen that carbon, nitrogen, lead and iodine are the main elements detected in the undoped sample. The atomic percentage and weight percentage of each element are reported in Figure 5.4 (a). The reported quantitative values are near to those obtained by Yao et al. [9] for undoped MAPI₃. Elemental mapping (Figure 5.4 (a)) shows that the elements well distributed throughout the surface.

From the EDS spectrum depicted in Figure 5.4 (b), the peak of K in the perovskite film is observable, indicating that the perovskite film contains potassium. The atomic percentage of the doped element was about 1%. The presence of potassium can also be detected by elemental mapping results in Figure 5.4 (b).

By adding 10 %wt. and 20 %wt. Sn to the potassium doped perovskite, the element was detected with EDS and elemental mapping analyses (Figure 5.5 (a) and (b)), and the detected atomic percentage and weight percentage of the element increased by increasing its concentration in the nanocomposite. These results prove the successful synthesis of perovskite structure doped by potassium as well as co-doped by different concentrations of tin elements, confirming the obtained results from other analyses.

5.3 XRD analysis

XRD peak profile analysis is a simple and powerful method to evaluate the peak broadening with crystallite size and lattice strain due to dislocation [10]. Figure 5.6 shows the X-ray diffraction patterns of the Methylammonium lead iodide (S) films before and after doping process with potassium (K) and different concentration of tin (10 and 20 %wt.) element.

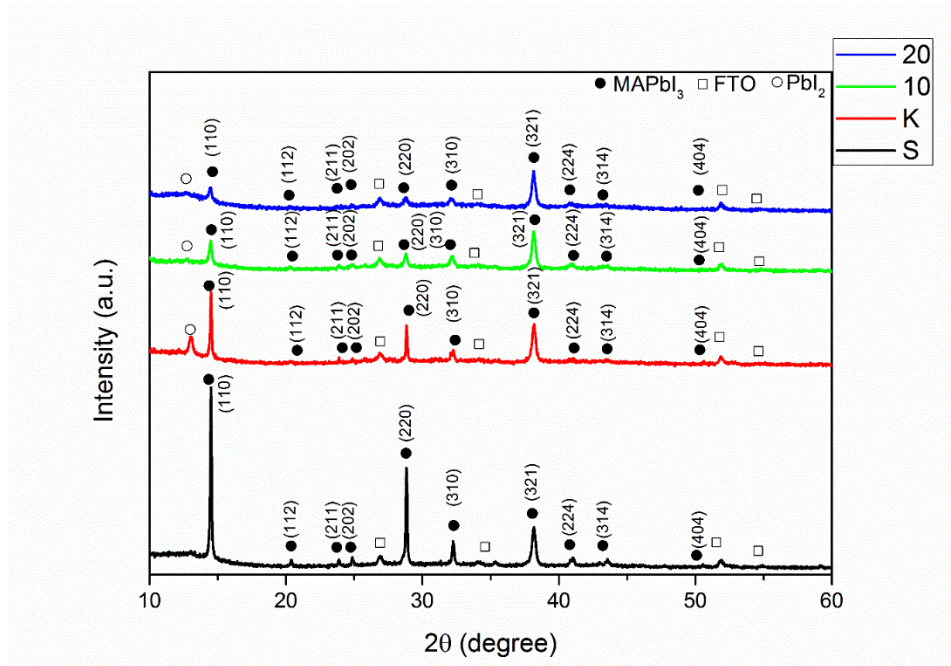


Figure 5.6: XRD patterns of the Methylammonium lead iodide (S) films before and after doping process with potassium (K) and different concentration of tin (10 and 20 %wt.) element.

It can be seen in the diffraction pattern of Methylammonium lead iodide thin film that there are the diffraction peaks around $2\theta = 14.5^\circ, 20.4^\circ, 23.8^\circ, 24.7^\circ, 28.8^\circ, 32.2^\circ, 35.3^\circ, 38.2^\circ, 41.0^\circ, 43.5^\circ, \text{ and } 50.5^\circ$, which can be assigned to the (110), (112), (211), (202), (220), (310), (321), (224), (314), and (404) planes of the tetragonal perovskite structure, respectively [11,12]. The indexing was performed by the relative combination of planar-spacing and Bragg's law, which determined the unit cell parameters from the peak positions [13]. In addition, some diffraction peaks of the substrate (FTO, JCPDS No. 77-0447) can be seen at $2\theta = 26.8^\circ$ (110), 34.0° (101), 51.8° (211), and 55.0° (220), due to the low thickness of the deposited layer.

From the XRD pattern of the potassium and tin doped samples, a peak of PbI_2 (JCPDS No. 07-0235) at 13° (001) can be seen in addition to the perovskite and FTO peaks, indicating the partly transformation of PbO to PbI_2 in the presence of the doped elements. The position of the peaks didn't change by doping the K element in the structure. However, by doping 10 and 20 %wt. of Sn in the structure, the position of the peaks shifted about 0.1° and 0.2° to lower values, respectively, confirmed successfulness of the doping process. The minor shifting of peaks towards the lower angle was due to the smaller ionic radius of Sn^{2+} (110 pm) than Pb^{2+} (119 pm) [14]. The narrow and sharp diffraction peaks showed high crystallinity and orientation [11]. So, the lower intensity and sharpness of the diffraction peaks in the doped samples indicates the reduction of the crystallinity of the system in the presence of the K and Sn elements. However, the intensity of the PbI_2 peak decreased in the presence of the tin element, indicating more conversion of PbI_2 to the MAPbI_3 structure.

The peak broadening of the XRD pattern can be used to estimate the lattice strain and crystallite size of the perovskite thin films. During the perovskite thin film growth, there is internal stress in the film. According to Williamson and Hall, the diffraction line broadening is due to crystallite size and contribution [15]. Generally, grain size (D) describes the diameter of each grain sediment. By contrast, dislocation line density (δ) describes the defects or irregularities of the crystalline structure. Where dislocation line density is used to calculate the number of flaws in a sample, a lower δ value means that the film is of higher quality [14]. The average crystallite size (D) can be obtained from the Debye-Scherrer

Equation (1), and the lattice strain (ϵ) was calculated by the following Williamson-Hall Equation (2) [16,17]. In addition Equation (3) was used to compute δ parameter [14].

$D = 0.89\lambda/\beta \cos(\theta)$	(1)
$\beta \cos(\theta)/\lambda = 1/D + \epsilon \sin(\theta)/\lambda$	(2)
$\delta = 1/D^2$	(3)

where λ is the wavelength of Cu-K α (1.5406 Å) radiation, β is full width at half maximum (FWHM) and θ is Bragg's angle.

The D, ϵ and δ of the pure MAPbI₃ film were 84.4 nm, 0.08% and $1.402 \times 10^{14} \text{ m}^{-2}$, respectively. When K was doped into MAPbI₃ film, D increased to 93.1 nm and ϵ and δ decreased to 0.07% and $1.151 \times 10^{14} \text{ m}^{-2}$. This indicated the appropriate lattice location of K atoms within the MAPbI₃ film structure. The D, ϵ , and δ of 10% Sn and 20% Sn co-doped MAPbI₃ films were 32.4 nm, 0.21% and $9.510 \times 10^{14} \text{ m}^{-2}$ and 26.15 nm, 0.26% and $1.462 \times 10^{15} \text{ m}^{-2}$, respectively. The decreasing trend of D and increasing trend of ϵ and δ values indicates a reduction in the film's crystal structure quality. This is due to the fact that there are extremely few substitutional sites accessible at this concentration. This supports the observations of Wang et al. [18] and Khan et al. [14], who discovered that doping significant amounts of Sn into MAPbI₃ films reduces grain size.

5.4 UV-Vis analysis

As the name implies, this spectrophotometer measures the interaction of light with solids or liquids in the UV-VIS regions. These regions are more interesting and important because different optical transitions in solids occur over these spectral intervals. The absorption spectra of samples are shown Figure 5.7.

According to Figure 5.7, all the considered films show roughly the same absorption edge at about 750 nm, which represents a usual feature in MAPbI₃ [19,20]. It can be seen that the absorbance in the UV-visible region enhances after doping the MAPbI₃ structure with potassium and tin elements as was seen in some other studies [6,7].

The optical bandgap (E_g) can be estimated by the Tauc equation [21]:

$$\alpha h\nu = A (h\nu - E_g)^n$$

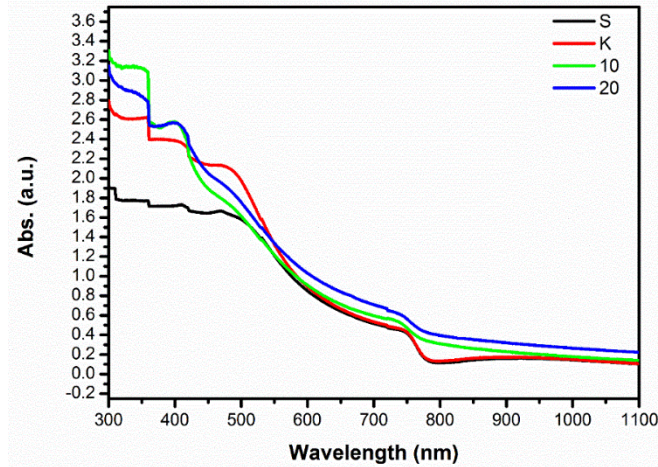


Figure 5.7: UV-Vis spectra of the Methylammonium lead iodide (S) films before and after doping process with potassium (K) and different concentration of tin (10 and 20 %wt.) element

where $h\nu$, α and A are the photon energy, absorption coefficient and constant, respectively; n has the value 0.5 and 2 for direct and indirect transition, respectively. Similarly, the value of the exponent represented as $n = 3/2$ for direct forbidden, and the value for indirect forbidden transitions $n = 3$, are utilized [14]. According to the literature, the optical absorption for this kind of perovskite occurs via direct transition [22,23]. The plots of $(\alpha h\nu)^2$ versus $h\nu$ are depicted in Figure 10 for all samples. The bandgap energy (E_g) was estimated from the intersection of extending the linear part of $(\alpha h\nu)^2$ with the abscissa $h\nu$.

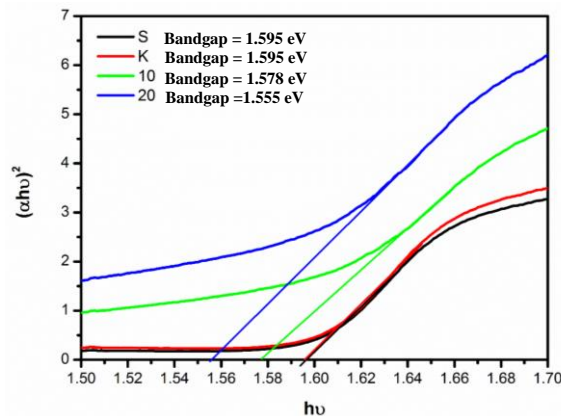


Figure 5.8: . Tauc plots of the Methylammonium lead iodide (S) films before and after doping process with potassium (K) and different concentration of tin (10 and 20 %wt.) element.

It is clear from Figure 5.8 that the bandgap energy for both undoped and K-doped samples was about 1.595 eV. It is in good agreement with obtained results by Zaman et al [7], where it was proved that there was no significant change in bandgap of K-doped perovskite sample, but absorption tends to increase, showing the K-doped sample is more suitable for solar absorption. The band gap energy value obtained for the pure MAPbI₃ agrees with both experimentally measured data ranging from 1.57 to 1.63 eV [20,24,25], and results from density functional theory (DFT) calculations [26]. In addition, it can be seen that by incorporation of 10 %wt. and 20 %wt. Sn in the perovskite structure the bandgap energy values decreased to about 1.578 eV and 1.555 eV, respectively. Sn has previously reduced the band gap in MAPbI₃ [14,27]. In fact, the Sn-containing samples decreases the apparent band gap because the Sn passivation is reducing the traps inside the MAPI₃ bandgap [27].

Furthermore, to probe the functional groups of the undoped and doped perovskite samples, FTIR measurements have been performed, and the obtained spectra are shown in Figure 5.9.

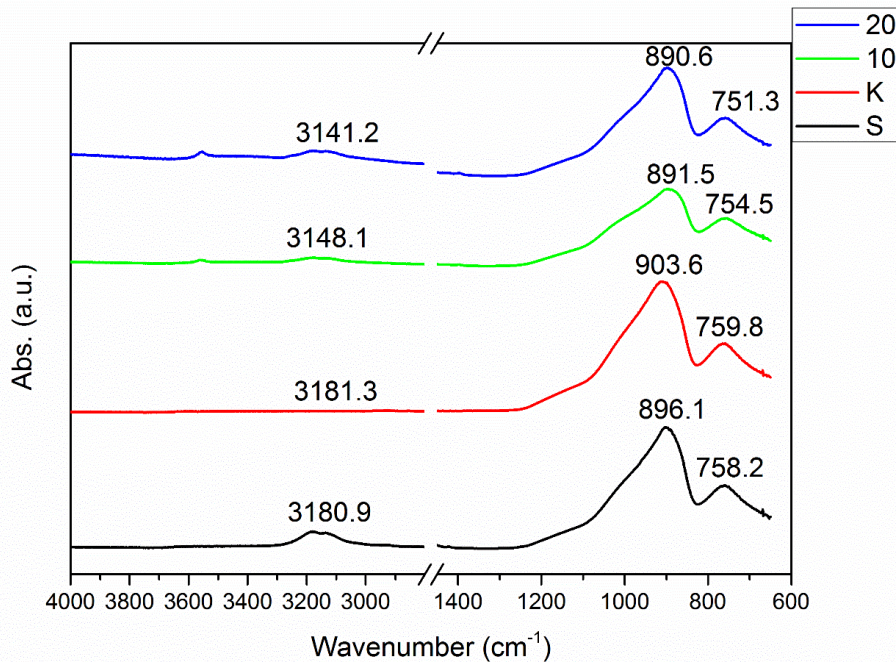


Figure 5.9: FTIR spectra of the Methylammonium lead iodide (S) films before and after doping process with potassium (K) and different concentration of tin (10 and 20 %wt.) element.

According to these spectra broad peaks can be seen at about 3140 cm^{-1} to 3180 cm^{-1} attributing to the asymmetric and symmetric mode of N–H stretching vibration associated with the NH^{3+} group of the MA cation [28]. The peaks at about 900 cm^{-1} and 760 cm^{-1} correspond to $\text{CH}_3\text{NH}^{3+}$ rocking modes, and N-H wagging vibration, respectively [28–30]. Doping of potassium and tin elements into the crystalline structure of the MAPI3-based perovskite, can affect the length of the bonds. In fact, in the case of K-doped PbI_3 , the introduction of potassium (K) atoms into the crystal lattice can alter the electronegativity of the compound compared to pure PbI_3 . Potassium (0.82) is less electronegative than lead (1.87). This means that potassium has a weaker ability to attract electrons towards itself in a chemical bond compared to lead. When potassium is introduced into the crystal lattice of PbI_3 , the electronegativity of the compound decreases due to the presence of the less electronegative potassium atoms. It means that the K doped PbI_3 has less attraction of electrons toward itself, and so the electrostatic attraction of the doped sample is more than the pure PbI_3 for $\text{CH}_3\text{NH}^{3+}$ resulting in the more required energy to vibrate the bonds (blue shift of the peak positions). On the other hand, in the presence of Sb (with an electronegativity of 1.96), the electrostatic attraction of the Sn-doped sample is less than the K-doped PbI_3 sample for $\text{CH}_3\text{NH}^{3+}$ resulting in the less required energy to vibrate the bonds (red shift of the peak positions).

5.5 PL spectroscopy

To understand the changes in electronic structure of the perovskite samples, PL emission spectroscopy was performed on the undoped and doped MAPbI_3 samples (Figure 5.10). It can be seen that the emission peaks of the four perovskite samples ranged from 800 nm to 850 nm.

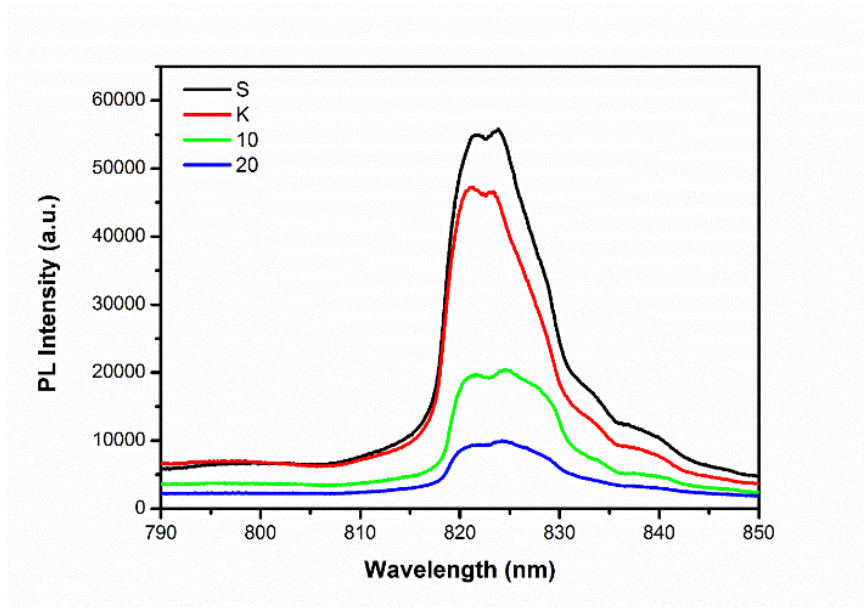


Figure 5.10: PL spectra of the Methylammonium lead iodide (S) films before and after doping process with potassium (K) and different concentration of tin (10 and 20 %wt.) element

According to Figure 4.10, the tetragonal MAPbI_3 possesses different PL features, with two or more peaks as was seen in literature [31–33]. Since the tetragonal MAPbI_3 is a direct-band-gap crystal, multiple PL peaks indicate that there are multiple radiative recombination centers involved, e.g., intrinsic defect states, extrinsic impurities, and residual orthorhombic MAPbI_3 crystals [31]. For the undoped sample the peak intensity of PL is high, indicating that the number of photo-generated carriers injected from the perovskite light-absorbing layer is the lowest. With doping of K^+ , the PL intensity of the perovskite sample decreased, and the number of photogenerated carrier injected to from the perovskite light-absorbing layer increased slightly. By doping 10% and 20% tin into the composite, the peak intensity decreased significantly, resulting in the more injection of photo-generated carriers from the perovskite light-absorbing layer in the presence of more tin element concentrations. Indeed, doping with potassium and tin ions can introduce additional trap states within the perovskite material, as well as formation of defects within the perovskite crystal structure. These trap states and defects act as non-radiative recombination centers, where excitons (electron-hole pairs) are captured and recombine without emitting light. This leads to a decrease in the intensity of the PL peak.

5.6 Contact angle measurements

To figure out the effect of the doping process on the hydrophobicity and stability of perovskite films, we also measured the static contact angle with water of the under-studied samples Figure 5.11.

From Figure 5.11, it is clear that the contact angle value increased slightly from about 9° for the pure MAPbI_3 to about 9.5° for the potassium doped sample. After doping 10 %wt. and 20 %wt. tin element in the K-doped MAPbI_3 sample, the contact angle increased to about 25.3° and 38.2° , respectively. It is well known that perovskite materials have a hydrophilic surface (as is shown in Figure 5.11 (a)) are highly sensitive to moisture, which can degrade their performance and stability [34,35]. Hydrophobicity helps to repel water and prevent its penetration into the perovskite layer, thus protecting the material from moisture-induced degradation. In addition, hydrophobic surfaces reduce the contact area between perovskite and water molecules, minimizing the chances of chemical reactions that could lead to material decomposition or ion migration. This improved stability is crucial for the long-term performance and durability of perovskite solar cells [36]. In fact, the doping process can improve the passivation of defects and grain boundaries on the perovskite surface. This passivation reduces the presence of reactive sites that can interact with water molecules, further enhancing the hydrophobicity of the material, that is in good agreement with some other researches [37,38]. This phenomenon can be related to the results of PL analysis, by considering on this fact that hydrophobic surfaces tend to have lower interfacial energy, reducing charge trapping and recombination at the interfaces, and enabling better charge transfer kinetics.

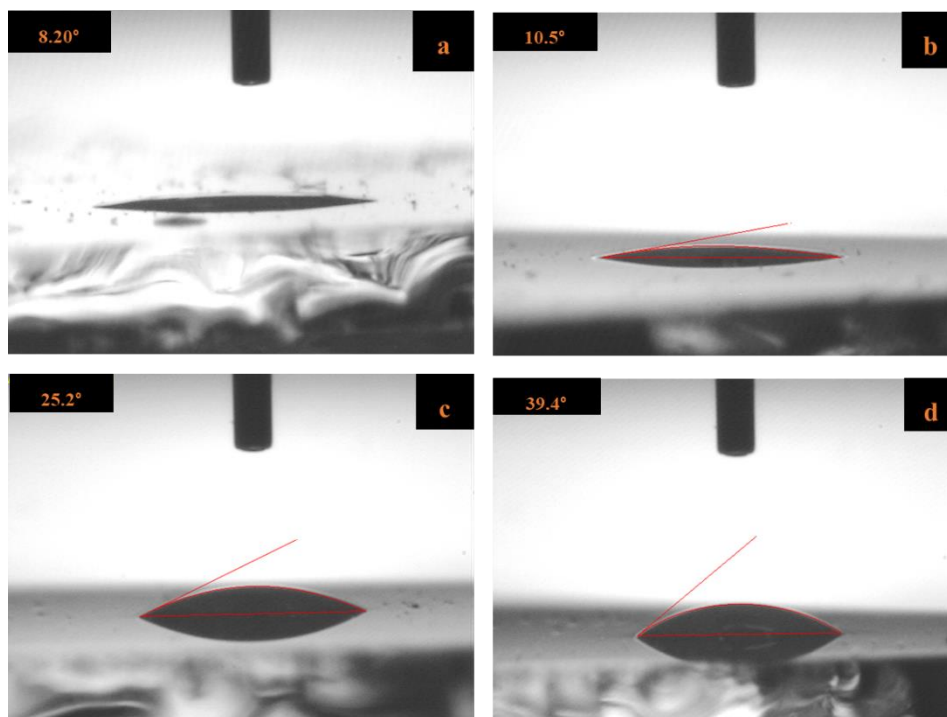


Figure 5.11: Contact angle photographs based on the following perovskite phase: (a) MAPbI₃, (b) MAPbI₃ doped with potassium, (c) MAPbI₃ doped with potassium and 10 %wt. Sn, and (d) MAPbI₃ doped with potassium and 20 %wt. Sn

References

- [1] Zhou Z, Wang Z, Zhou Y, Pang S, Wang D, Xu H, et al. Methylamine-Gas Induced Defect-Healing Behavior of CH₃NH₃PbI₃ Thin Films for Perovskite Solar Cells. *Angew Chem Int Ed Engl* 2015;54. doi:10.1002/anie.201504379.
- [2] Mehdi H, Leonat LN, Stancu V, Saidi H, Enculescu M, Tomulescu A-G, et al. Effect of chlorine and bromine on the perovskite crystal growth in mesoscopic heterojunction photovoltaic device. *Mater Sci Semicond Process* 2022;143:106558. doi:https://doi.org/10.1016/j.mssp.2022.106558.
- [3] Pineda De La O E, Alhazmi N, Ebbens SJ, Dunbar ADF. Influence of Additives on the In Situ Crystallization Dynamics of Methyl Ammonium Lead Halide Perovskites. *ACS Appl Energy Mater* 2021;4:1398–409. doi:10.1021/acsaem.0c02625.
- [4] Xu F, Zhang T, Li G, Zhao Y. Synergetic Effect of Chloride Doping and CH₃NH₃PbCl₃ on CH₃NH₃PbI₃-xCl_x Perovskite Based Solar Cells. *ChemSusChem* 2017;10. doi:10.1002/cssc.201700487.
- [5] Singh R, Sharma P, Lu C-H, Kumar R, Jain N, Singh J. Structural, morphological and thermodynamic parameters investigation of tunable MAPb_{1-x}Cd_xBr_{3-2x}I_{2x} hybrid perovskite. *J Alloys Compd* 2021;866:158936. doi:10.1016/j.jallcom.2021.158936.
- [6] Liu D, Guo Y, Yang Y, Liu J, Yin X, Que W. CuInSe₂ quantum dots doped MAPbI₃ films with reduced trap density for perovskite solar cells. *J Alloys Compd* 2022;906:164292. doi:https://doi.org/10.1016/j.jallcom.2022.164292.
- [7] Muzammal uz Zaman M, Imran M, Saleem A, Kamboh AH, Arshad M, Khan NA, et al. Potassium doped methylammonium lead iodide (MAPbI₃) thin films as a potential absorber for perovskite solar cells; structural, morphological, electronic and optoelectric properties. *Phys B Condens Matter* 2017;522:57–65. doi:https://doi.org/10.1016/j.physb.2017.07.067.
- [8] Hou X, Huang sm, Ou-Yang W, Pan L, Sun Z, Chen X. Constructing Efficient and Stable Perovskite Solar Cells via Interconnecting Perovskite Grains. *ACS Appl Mater Interfaces* 2017;9. doi:10.1021/acsaami.7b08488.

- [9] Yao E, Zou, Cheng N-C, Ling, Chang, Chen W. Impact of K⁺ Doping on Modulating Majority Charge Carrier Type and Quality of Perovskite Thin Films by Two-step Solution Method for Solar Cells. *Coatings* 2019;9:647. doi:10.3390/coatings9100647.
- [10] Javidparvar AA, Mosavi MA, Ramezanzadeh B. Nickel-aluminium bronze (NiBRAl) casting alloy tribological/corrosion resistance properties improvement via deposition of a Cu-doped diamond-like carbon (DLC) thin film; optimization of sputtering magnetron process conditions. *Mater Chem Phys* 2023;296:127279. doi:10.1016/J.MATCHEMPHYS.2022.127279.
- [11] Li X, Chen Y, Li L, Huang J. Perovskite Thin Film Consisting with One-Dimensional Nanowires. *Materials (Basel)* 2018;11:1–14. doi:10.3390/ma11091759.
- [12] Mirhendi SM, Golobostanfard MR, Abdizadeh H. Effect of Speed of Spin Coating Deposition on Properties of CH₃NH₃PbI₃ Organic-Inorganic Halide Perovskite. *2nd Int. Conf. Ceram.*, 2017.
- [13] Ong KP, Goh TW, Xu Q, Huan A. Structural Evolution in Methylammonium Lead Iodide CH₃NH₃PbI₃. *J Phys Chem A* 2015;119:11033–8. doi:10.1021/ACS.JPCA.5B09884/SUPPL_FILE/JP5B09884_SI_001.PDF.
- [14] Properties P, Solar P, Almuqrin AH, Almoneef MM, Iqbal M. Bi and Sn Doping Improved the Structural, Optical and Photovoltaic Properties of MAPbI₃ -Based Perovskite Solar Cells. *Materials (Basel)* 2022;15:1–12.
- [15] Thanikaikarasan S, Dhanasekaran D, Sankaranarayanan K. Electrochemical, structural, compositional and optical properties of Cuprous Selenide thin films. *Chinese J Phys* 2020;63:138–48. doi:10.1016/J.CJPH.2019.10.023.
- [16] Chaki SH, Malek TJ, Deshpande MP. Magnetite Fe₃O₄ nanoparticles synthesis by wet chemical reduction and their characterization. *Adv Nat Sci Nanosci Nanotechnol* 2015;6:1–6. doi:10.1088/2043-6262/6/3/035009.
- [17] Hajipour F, Asad S, Amoozegar MA, Javidparvar AA, Tang J, Zhong H, et al. Developing a fluorescent hybrid nanobiosensor based on quantum dots and azoreductase enzyme formethyl red monitoring. *Iran Biomed J* 2021;25. doi:10.29252/ibj.25.1.8.

- [18] Wang S, Zhao K, Shao Y, Xu L, Huang YP, Li W. Evolutions of optical constants, interband electron transitions, and bandgap of Sn-doped CH₃NH₃PbI₃ perovskite films. *Appl Phys Lett* 2020;116:3–8. doi:10.1063/5.0007293.
- [19] Kitazawa N, Watanabe Y, Nakamura Y. Optical properties of CH₃NH₃PbX₃ (X= halogen) and their mixed-halide crystals. *J Mater Sci* 2002;37:3585–7.
- [20] Colella S, Mosconi E, Fedeli P, Listorti A, Gazza F, Orlandi F, et al. MAPbI₃-xCl_x mixed halide perovskite for hybrid solar cells: the role of chloride as dopant on the transport and structural properties. *Chem Mater* 2013;25:4613–8.
- [21] Singh L, Singh Samra K, Singh R. Opto-chemical response of CR-39 and polystyrene to swift heavy ion irradiation. *Nucl Instruments Methods Phys Res Sect B Beam Interact with Mater Atoms* 2007;255:350–6. doi:10.1016/j.nimb.2006.11.129.
- [22] Navas J, Sánchez-Coronilla A, Gallardo JJ, Hernández NC, Piñero JC, Alcántara R, et al. New insights into organic--inorganic hybrid perovskite CH₃NH₃PbI₃ nanoparticles. An experimental and theoretical study of doping in Pb²⁺ sites with Sn²⁺, Sr²⁺, Cd²⁺ and Ca²⁺. *Nanoscale* 2015;7:6216–29.
- [23] Hsieh CM, Yu YL, Chen CP, Chuang SC. Effects of the additives: N -propylammonium or n -butylammonium iodide on the performance of perovskite solar cells. *RSC Adv* 2017;7:55986–92. doi:10.1039/c7ra11286f.
- [24] Qiu J, Qiu Y, Yan K, Zhong M, Mu C, Yan H, et al. All-solid-state hybrid solar cells based on a new organometal halide perovskite sensitizer and one-dimensional TiO₂ nanowire arrays. *Nanoscale* 2013;5:3245–8.
- [25] Noh JH, Im SH, Heo JH, Mandal TN, Seok S II. Chemical management for colorful, efficient, and stable inorganic-organic hybrid nanostructured solar cells. *Nano Lett* 2013;13:1764–9.
- [26] Mosconi E, Amat A, Nazeeruddin MK, Gratzel M, De Angelis F. First-principles modeling of mixed halide organometal perovskites for photovoltaic applications. *J Phys Chem C* 2013;117:13902–13.

- [27] Zou Y, Guo R, Buyruk A, Chen W, Xiao T, Yin S, et al. Sodium dodecylbenzene sulfonate interface modification of methylammonium lead iodide for surface passivation of perovskite solar cells. *ACS Appl Mater Interfaces* 2020;12:52643–51.
- [28] Maity S, Lokku VK, Lata A, Sarkar K, Ahmed J, Majeed Khan MA, et al. MAPbI₃-based efficient, transparent and air-stable broadband photodetectors. *Indian J Phys* 2022;96:903–8. doi:10.1007/s12648-020-02004-x.
- [29] Yerezhap D, Omarova Z, Aldiyarov A, Shinbayeva A, Tokmoldin N. IR Spectroscopic Degradation Study of Thin Organometal Halide Perovskite Films. *Molecules* 2023;28. doi:10.3390/molecules28031288.
- [30] Abdelmageed G, Jewell L, Hellier K, Seymour L, Luo B, Bridges F, et al. Mechanisms for light induced degradation in MAPbI₃ perovskite thin films and solar cells. *Appl Phys Lett* 2016;109:233905. doi:10.1063/1.4967840.
- [31] Kong W, Ye Z, Qi Z, Zhang B, Wang M, Rahimi-Iman A, et al. Characterization of an abnormal photoluminescence behavior upon crystal-phase transition of perovskite CH₃NH₃PbI₃. *Phys Chem Chem Phys* 2015;17. doi:10.1039/C5CP02605A.
- [32] Chen Y, Wang T, Li Z, Li H, Ye T, Wetzel C, et al. Communicating Two States in Perovskite Revealed by Time-Resolved Photoluminescence Spectroscopy. *Sci Rep* 2018;8. doi:10.1038/s41598-018-34645-8.
- [33] Halder A, Chulliyil R, Subbiah A, Khan T, Chatteraj S, Chowdhury A, et al. Pseudohalide (SCN⁻)-doped MAPbI₃ perovskites: A few surprises. *J Phys Chem Lett* 2015;6. doi:10.1021/acs.jpcclett.5b01327.
- [34] Hwang I, Jeong I, Lee J, Ko MJ, Yong K. Enhancing Stability of Perovskite Solar Cells to Moisture by the Facile Hydrophobic Passivation. *ACS Appl Mater Interfaces* 2015;7:17330–6. doi:10.1021/acsami.5b04490.
- [35] Poli I, Liang X, Baker R, Eslava S, Cameron PJ. Enhancing the hydrophobicity of perovskite solar cells using C18 capped CH₃NH₃PbI₃ nanocrystals. *J Mater Chem C* 2018;6:7149–56. doi:10.1039/C8TC01939H.

- [36] Xia J, Liang C, Mei S, Gu H, He B, Zhang Z, et al. Deep surface passivation for efficient and hydrophobic perovskite solar cells. *J Mater Chem A* 2021;9:2919–27. doi:10.1039/D0TA10535J.
- [37] Luo J, Lin F, Xia J, Yang H, Zhang R, Malik HA, et al. An efficient and hydrophobic molecular doping in perovskite solar cells. *Nano Energy* 2021;82:105751. doi:<https://doi.org/10.1016/j.nanoen.2021.105751>.
- [38] Yu C, Zhang B, Chen C, Wang J, Zhang J, Chen P, et al. Stable and highly efficient perovskite solar cells: Doping hydrophobic fluoride into hole transport material PTAA. *Nano Res* 2022;15:4431–8. doi:10.1007/s12274-021-4056-x.

Chapter 6

Conclusion and Future Recommendations

The chapter presents and concludes the findings from the conducted research. Moreover, for further exploration and analysis future recommendations are also given.

6.1 Conclusion

In a nutshell, brief introduction of light harvesting through solar cell has been described along with detailed structure and working mechanism of Perovskite Solar Cell. Perovskite absorber layer as the core of the cell absorbs the photons and convert them into electrical energy. An extensive literature review on compositional engineering of perovskite absorber layer has been conducted and use of different elements and their effects has been studied. Along with that use of different additives particularly Sn-powder has been discussed.

Keeping in view the literature, precursor solutions for various compositions were prepared and then deposited using two step deposition process in an ambient environment. The samples were then characterized using SEM, XRD, UV vis, PL and Contact angle measurements. From the results it has been observed that Sn doping improves absorption and hole mobilities. With the increased doping of Sn, grain size has been reduced. UV results illustrated the enhanced light absorption with the same bandgap for K as a dopant. Bandgap bowing has occurred due to the doping of Sn.

6.2 Future Recommendations

Following are the some of the recommendations for future research:

- i. Analysis and study at different concentrations of potassium doping.
- ii. Sn doping at a higher concentration and its effect on the morphology and optoelectrical properties of the layer can be studied.
- iii. Use of additives other than Sn power such as Guanidinium thiocyanate (GuaSCN), Polyethylene glycol (PEG) and caffeine can be studied.

- iv. Characterization techniques such as XPS, AFM, TEM and EQE can be performed to better understand the working of the layer.
- v. Cell formation.

Journal Publication

Optimizing optoelectronic properties of Perovskite Absorber Material via ambient compositional engineering with Potassium (K)

Muhammad Usman Nawaz^a, *Nadia Shahzad^a, Muhammad Salik Qureshi^a, Naseem Iqbal^a, Majid Ali^a, Muhammad Imran Shahzad^b

^a*U.S.-Pakistan Centre for Advanced Studies in Energy (USPCAS-E), National University of Sciences & Technology (NUST), H-12 Sector (44000) Islamabad, Pakistan*

^b*Nanosciences and Technology Department (NS&TD), National Centre for Physics (NCP), 44000 Islamabad, Pakistan*

*Corresponding Author's Email: nadia@uspcase.nust.edu.pk

Abstract

Perovskite solar cells (PSCs) have emerged as a promising contender for next-generation photovoltaic technology due to their remarkable light-harvesting capabilities and cost-effectiveness. However, challenges such as lead toxicity, Sn oxidation, and the instability of organic Methylammonium (MA) have hindered their widespread adoption. In this study, we address these issues by investigating the potential and stability of MAPbI₃ through the doping of potassium (K) and tin (Sn) in an ambient environment. To tackle MA instability, we partially introduce K into the A site, while Sn powder facilitates a comproportionating reaction to counter Sn⁺⁴ oxidation, effectively addressing the stability concerns. Systematic experimentation revealed that doping K and Sn in the A and B sites of MAPbI₃ leads to a reduction in grain size and Sn vacancies, along with increased light absorption. K doping maintains the bandgap, while Sn doping results in a reduced bandgap. Additionally, the incorporation of Sn powder yields a more uniform and high-quality perovskite film, exhibiting improved optoelectronic properties. Remarkably, doped films demonstrate an increase in photogenerated electrons and more hydrophobic layer. These findings represent a significant advancement in perovskite technology, offering the great potential for more environmentally friendly, stable and even applicable in tandem solar cells.

Keywords: Perovskite Solar Cells, Sn-Pb based perovskite, potassium and tin doping, compositional engineering, ambient fabrication.